The Eshelby problem of the confocal N-layer spheroid with imperfect interfaces and the notion of equivalent particle in thermal conduction

Jean-François Barthélémy, François Bignonnet

The Eshelby problem of the confocal N-layer spheroid with imperfect interfaces and the notion of equivalent particle in thermal conduction

J.-F. Barthélémy[a,*], F. Bignonnet[b]

[a] *Cerema, Project-team DIMA, 110 rue de Paris, BP 214, 77487 Provins Cedex, France*
[b] *GeM, Research Institute of Civil Engineering and Mechanics, UMR CNRS 6183, Université de Nantes, France*

Abstract

The solution to the generalized conduction Eshelby problem of a confocal N-layer spheroid with low or highly conducting interfaces between isotropic layers is provided thanks to a decomposition in series of harmonics. A generic workflow is detailed for practical numerical implementation including a fine analysis to assess the influence of the level of truncation of the infinite series. The case of perfect interfaces presents a particular interest insofar as it is characterized by an equivalent conductivity tensor obtained from a recursive procedure. The notion of equivalent conductivity is then investigated and applied to a uniform spheroid surrounded by an imperfect interface. Some approximated models are developed, either based on a surface description of the interface or on a thin interphase, casting a new light on published models and proposing a unified framework for new ones. These approximated models are finally analyzed by comparison to the exact solution.

Keywords:
Eshelby problem, conductivity, n-layer spheroid, imperfect interface, equivalent particle

1. Introduction

Relating the specificities of the macroscopic behavior of materials to the responsible mechanisms and microstructure at the lower scales has become an important issue in the field of material research and engineering in the last decades. Indeed a better understanding of the behavior of materials and their evolution with time (aging, damage,...) often requires to investigate their lower scale characteristics which may in turn open a way for a control of the macroscopic properties by optimization of the microstructure (in civil engineering, aeronautics...). The homogenization techniques allowing to build relationships between the microscopic geometrical and physical properties and the macroscopic properties of materials (such as elasticity, strength, thermal or electrical conduction, ionic diffusion, permeability...) have shown to be prominent tools in this context [1].

After Eshelby's pionnering work [2] allowing to build models of homogenization in which heterogeneities and phase distributions are described as ellipsoids, the generalization of the fundamental problem of a particle embedded in an infinite matrix to the case of complex heterogeneities has been given an important place in many research topics. For instance the notion of composite sphere assemblage [3], the three-phase model [4] generalized in [5] to an arbitrary number of layers have put in evidence the benefits brought by a generalization of the Eshelby problem to an elastic N-layer sphere for which a solution had been provided earlier by Love [6]. More generally the idea of morphologically representative pattern has allowed to enrich estimates or bounds of elastic moduli ([7], [8]) even if sometimes analytical solutions seem out of reach and numerical techniques have to be used ([9], [10], [11], [12]). The N-layer sphere pattern has also been considered in the framework of thermal conduction [13]. Moreover in order to get closer to the actual physics taking place around heterogeneities or pores (membrane effect around nanopores, localized electrical

*Corresponding author
Email addresses: jf.barthelemy@cerema.fr (J.-F. Barthélémy), francois.bignonnet@univ-nantes.fr (F. Bignonnet)

flux around conductors, diffusive flux around aggegates, thermal barriers...) some models have taken into account the presence of interfaces around spherical particles ([14], [15], [16]). Other works have investigated the opportunity to consider spheroidal or even any ellipsoidal shapes in a multilayer particle through approximated models based on Green techniques ([17] and [18] for elasticity and [19] for thermal conduction). The case of a uniform spheroidal or even ellipsoidal particle surrounded by an imperfect interface (low or highly conducting interface in conduction or stiff or compliant interface in elasticity) or by an interphase has also particularly been focusing the attention for some time. Indeed exact solutions based on decompositions in harmonics have been found in conduction ([20], [21], [22]) or in elasticity ([23], [24], [25], [26]). However these solutions require rather tedious mathematical developments, inciting then several authors to propose simpler approximated models which may in addition have the advantage to apply to anisotropic constituents whereas the analytical solutions are often constrained to isotropic ones. As regards conduction, some approximated models rely on a surface description of the interface and its properties ([27], [28], [29], [30], [31]) whereas some others consider the interface as the limit case of a thin interphase ([32], [33], [34], [35]). It is worth noting that the same kind of considerations about the description of interface and the construction of simplified models can be found in the framework of elasticity ([36], [37], [38]).

The present contribution aims at casting a new light on the notion of equivalent conductivity in the case of a composite spheroidal particle possibly presenting several layers and imperfect interfaces between layers. The issue of the determination of such a property is a preliminary step eventually followed by the implementation of homogenization schemes which are not addressed in this work. To begin with, it seems interesting to unfold an analytical solution which can be obtained in the case of a confocal multilayer spheroid with imperfect interfaces in such a way that a practical implementation is facilitated and convergence problems arising from the formulation are properly investigated. This analytical solution has both the advantages to appear as a reference solution for approximated models of coated spheroids and to provide instructive results in terms of equivalent conduction in presence of perfect interfaces. Thanks to its relative simplicity the case of a uniform spheroidal particle surrounded by an imperfect interface is an interesting example for which the concept of equivalent conductivity still deserves new clarifications beyond already published results.

The paper falls into three parts. The first one (section 2) corresponds to the explicit resolution of the generalized conduction Eshelby problem of a confocal multilayer spheroid with imperfect interfaces between layers. A particular attention is paid to the calculation details and justifications which are necessary for a numerical implementation. The second part (section 3) consists in a specific focus on the confocal multilayer spheroid with perfect interfaces which presents some interesting particularities allowing to introduce the concept of equivalent inclusion. The latter is the topic of the third part (section 4) developing some general considerations and discussion about its validity and leading to its application to the case of a uniform spheroid surrounded by an imperfect interface. The latter problem has already been tackled in the literature and the present framework allows to recover efficiently some existing approximated models revisited under the point of view of the equivalent conductivity. A new formulation of approximated models is finally proposed and a comparison between models is carried out.

2. General resolution of the confocal N-layer spheroid problem in thermal conduction

This section is devoted to the determination of the generalized Eshelby solution of a confocal N-layer spheroid particle with imperfect interfaces in the framework of second-order elliptic problems. In the sequel, the terminology of thermal conductivity is used but all the results can be transposed to diffusion, electrical conductivity, dielectric permittivity, permeability... Initially based on some already known results concerning the use of series of spherical and spheroidal harmonics ([39], [40], [41]) in problems involving spheroidal particles with interfaces ([20], [21], [22], [42]), this section aims at extending them to a multilayer particle. The approach is inspired by previous works dealing with the elastic spherical case ([5], [16]) or the conductive spherical case [13] with a particular focus on practical implementation made more complex by the presence of infinite series of harmonics and numerical issues that may arise along the calculation of the latter.

2.1. Description of the problem and general form of the solution

The generalized Eshelby problem at stake here relies on a confocal N-layer spheroid particle, each layer Ω_ℓ ($1 \leq \ell \leq N$) corresponding to a uniform conductive material, embedded in an infinite matrix Ω_{N+1}. The geometry is represented in figure 1 where the prolate (resp. oblate) case is obtained by symmetry of revolution around the vertical (resp. horizontal) axis.

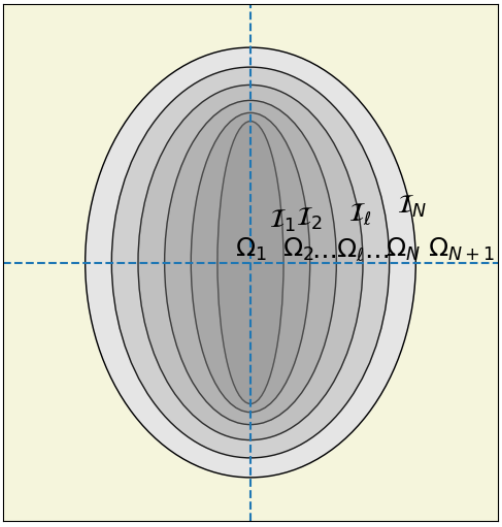

Figure 1: Confocal N-layer spheroid embedded in an infinite matrix

In the following developments the expressions are given in the prolate spheroidal coordinates (φ, p, q) from which their oblate counterparts can be retrieved from a simple parameter replacement (see AppendixA for notations and details concerning spheroidal coordinates). The conductivity within Ω_ℓ ($1 \leq \ell \leq N+1$) is assumed isotropic $\boldsymbol{k}_\ell = k_\ell \mathbf{1}$ and the interface between Ω_ℓ and $\Omega_{\ell+1}$ denoted by $\mathcal{I}_\ell$ (mathematically defined by a levelset of equation $q = q_\ell$ with $q_{\ell+1} > q_\ell > 1$) follows one of the three types of characteristic adopting the terminology employed in [42]: perfect interface (P), low conducting interface (LC) also called Kapitza model of interface thermal resistance α_ℓ [43] or highly conducting interface (HC) of surface conductivity β_ℓ. The whole system $\Omega = \mathbb{R}^3 = \cup_{\ell=1}^{N+1} \Omega_\ell$ is subjected to a remote boundary condition of uniform temperature gradient $\underline{H}$. The set of equations of the steady state thermal problem is then given by

$$
\begin{cases}
\operatorname{div} \underline{u} = 0 \quad \text{in } \Omega & \text{(1a)} \\
\underline{u} = -k_\ell \, \underline{h} \quad ; \quad \underline{h} = \underline{\operatorname{grad}} \, T \quad \text{in } \Omega_\ell & \text{(1b)} \\
[\![T]\!] = 0 \quad \text{and} \quad [\![\underline{u}]\!] \cdot \underline{e}_q = 0 \quad \text{on } \mathcal{I}_\ell \text{ of P type} & \text{(1c)} \\
[\![T]\!] = -\alpha_\ell \, \underline{u} \cdot \underline{e}_q \quad \text{and} \quad [\![\underline{u}]\!] \cdot \underline{e}_q = 0 \quad \text{on } \mathcal{I}_\ell \text{ of LC type} & \text{(1d)} \\
[\![T]\!] = 0 \quad \text{and} \quad [\![\underline{u}]\!] \cdot \underline{e}_q = \beta_\ell \, \Delta_{\mathcal{S}} T \quad \text{on } \mathcal{I}_\ell \text{ of HC type} & \text{(1e)} \\
T \underset{\|\underline{x}\| \to \infty}{\sim} \underline{H} \cdot \underline{x} & \text{(1f)}
\end{cases}
$$

where T and $\underline{u}$ denote the temperature and heat flux fields, $[\![\mathcal{X}]\!] = \mathcal{X}_{\ell+1} - \mathcal{X}_\ell$ the discontinuity of an arbitrary field $\mathcal{X}$ across $\mathcal{I}_\ell$ and $\Delta_{\mathcal{S}}$ the surface Laplacian (A.11).

By linearity of the equations involved in the system (1a)-(1f), the temperature gradient and velocity fields are related to the remote temperature gradient $\underline{H}$ by means of concentration tensor fields $\boldsymbol{A}(\underline{x})$ and $\boldsymbol{B}(\underline{x})$ such that

$$
\underline{h} = \underline{\operatorname{grad}} \, T = \boldsymbol{A} \cdot \underline{H} \quad ; \quad \underline{u} = -\boldsymbol{B} \cdot \underline{H} \tag{2}
$$

The knowledge of $\boldsymbol{A}(\underline{x})$ and $\boldsymbol{B}(\underline{x})$ relies then on the complete resolution of the system (1a)-(1f) as performed hereafter. Moreover it is worth mentioning here that the averages of these tensors over any spheroid $\mathcal{E}_\ell$ bounded by $\mathcal{I}_\ell$ ($\mathcal{E}_\ell = \cup_{\lambda=1}^{\ell} \Omega_\lambda$), denoted by $< \boldsymbol{A} >_{\mathcal{E}_\ell}$ and $< \boldsymbol{B} >_{\mathcal{E}_\ell}$, are of crucial importance in upscaling techniques and in particular the averages over $\mathcal{E}_N$ which are directly involved in many homogenization schemes relying on auxiliary (generalized) Eshelby problems (e.g. Mori-Tanaka, self-consistent,...) providing estimates of composites incorporating a family of confocal N-layer spheroids. That is why the identification of these tensors is considered in the next sections.

Due to the isotropy of the conductivity in each layer, the combination of (1a) together with (1b) implies that the restriction of the temperature field to the domain Ω_ℓ, which is denoted by T_ℓ, is harmonic and can therefore be decomposed as an infinite sum of spheroidal harmonics ([39], [41]):

$$\begin{aligned} T_\ell = c \sum_{m=0}^{+\infty} \sum_{n=m}^{+\infty} P_n^m(p) \quad & \left\{ \left[a_{\ell,n}^m \, P_n^m(q) + b_{\ell,n}^m \, Q_n^m(q) \right] \cos(m\varphi) \right. \\ & \left. + \left[c_{\ell,n}^m \, P_n^m(q) + d_{\ell,n}^m \, Q_n^m(q) \right] \sin(m\varphi) \right\} \end{aligned} \tag{3}$$

where P_n^m and Q_n^m denote the associated Legendre functions of degree n and order m of respectively the first and second kinds (see AppendixB) and $a_{\ell,n}^m$, $b_{\ell,n}^m$, $c_{\ell,n}^m$ and $d_{\ell,n}^m$ the coefficients applying in Ω_ℓ. These coefficients have to be determined in consistency with the system (1a)-(1f). The terms $P_n^m(p)P_n^m(q)\cos(m\varphi)$ and $P_n^m(p)P_n^m(q)\sin(m\varphi)$ have finite limits in the vicinity of $q = 1$ and are called the regular harmonics whereas $P_n^m(p)Q_n^m(q)\cos(m\varphi)$ and $P_n^m(p)Q_n^m(q)\sin(m\varphi)$ have infinite limits when q tends towards 1 and are called the irregular harmonics. Noticeably the interface relationships (1c)-(1e) not only involve the expressions of T in successive layers but also the normal flux at the interface written in the ℓ^{th} layer as

$$\begin{aligned} \underline{u}_\ell \cdot \underline{e}_q \quad &= -\frac{k_\ell}{\chi_q} \frac{\partial T_\ell}{\partial q} \\ &= -\frac{k_\ell \sqrt{q^2-1}}{\sqrt{q^2-p^2}} \sum_{m=0}^{+\infty} \sum_{n=m}^{+\infty} P_n^m(p) \quad \left\{ \left[a_{\ell,n}^m \, P_n^{m'}(q) + b_{\ell,n}^m \, Q_n^{m'}(q) \right] \cos(m\varphi) \right. \\ & \qquad \left. + \left[c_{\ell,n}^m \, P_n^{m'}(q) + d_{\ell,n}^m \, Q_n^{m'}(q) \right] \sin(m\varphi) \right\} \end{aligned} \tag{4}$$

(4) is meant to be applied at $q = q_{\ell-1}$ or q_ℓ depending on whether it corresponds to the external flux at $\mathcal{I}_{\ell-1}$ or internal flux at $\mathcal{I}_\ell$.

For further interest and thanks to the Stokes theorem, the decomposition (3) is well adapted to calculate the average of $\underline{\text{grad}}\, T$ over $\mathcal{E}_\ell$ of volume $|\mathcal{E}_\ell| = \frac{4}{3}\pi c^3 q_\ell (q_\ell^2 - 1)$. Indeed observing that $p = P_1(p)$ and $\sqrt{1-p^2} = -P_1^1(p)$ since $|p| \leq 1$ and exploiting the expressions of $\underline{e}_q$ in (A.6) and $\mathrm{d}S_q$ in (A.7), it comes that

$$\begin{aligned} < \underline{h} >_{\mathcal{E}_\ell} \quad &= \tfrac{1}{|\mathcal{E}_\ell|} \int_{\partial\mathcal{E}_\ell} T_{\lambda_{|q=q_\ell}} \, \underline{e}_q \, \mathrm{d}S_q \\ &= \tfrac{3}{4\pi q_\ell \sqrt{q_\ell^2-1}} \int_{p=-1}^{1} \int_{\varphi=0}^{2\pi} \tfrac{T_{\lambda_{|q=q_\ell}}}{c} \left(-P_1^1(p)\, q_\ell \, \underline{u}_\varphi + P_1(p) \sqrt{q_\ell^2-1}\, \underline{e}_3 \right) \mathrm{d}\varphi \, \mathrm{d}p \end{aligned} \tag{5}$$

where $\lambda = \ell + 1$ if the interface is included in the average and $\lambda = \ell$ if it is not. In other words, in the case of LC interface involving temperature discontinuities, T_λ in (5) is taken equal to T_ℓ at $q = q_\ell$ if the interface is not considered in the averaging process or equal to $T_{\ell+1}$ at $q = q_\ell$ if the interface contributes to the average. In any other case (P or HC), the choice of T as T_ℓ or $T_{\ell+1}$ at $q = q_\ell$ is indifferent but can be motivated by the interest to express the result with respect to the coefficients of one or the other layer. Finally (5) can be simplified by introducing T (3), $\underline{u}_\varphi$ (A.2) and invoking the orthogonality condition (B.1f) as well as the definitions $P_1(q) = q$ and $P_1^1(q) = \sqrt{q^2-1}$ for $q > 1$:

$$< \underline{h} >_{\mathcal{E}_\ell} = -\left(a_{\lambda,1}^1 + b_{\lambda,1}^1 \, \mathcal{T}_t(q_\ell) \right) \underline{e}_1 - \left(c_{\lambda,1}^1 + d_{\lambda,1}^1 \, \mathcal{T}_t(q_\ell) \right) \underline{e}_2 + \left(a_{\lambda,1}^0 + b_{\lambda,1}^0 \, \mathcal{T}_a(q_\ell) \right) \underline{e}_3 \tag{6}$$

with

$$\mathcal{T}_t(q) = \frac{Q_1^1(q)}{\sqrt{q^2-1}} = \operatorname{arccoth} q - \frac{q}{q^2-1} \quad ; \quad \mathcal{T}_a(q) = \frac{Q_1(q)}{q} = \operatorname{arccoth} q - \frac{1}{q} \tag{7}$$

Besides, thanks to (1a) and using $\mathrm{d}S_q$ in (A.7) and $\underline{x}$ in (A.3), the average of $\underline{u}$ over $\mathcal{E}_\ell$ can also be obtained by a surface integral involving (4)

$$\begin{aligned} <\underline{u}>_{\mathcal{E}_\ell} &= \tfrac{1}{|\mathcal{E}_\ell|} \int_{\partial\mathcal{E}_\ell} \underline{x}\,(\underline{u}_\lambda \cdot \underline{e}_q)_{|q=q_\ell}\ \mathrm{d}S_q \\ &= \tfrac{-3\,k_\lambda}{4\pi\,q_\ell} \int_{p=-1}^{1}\int_{\varphi=0}^{2\pi} \tfrac{\partial(T_\lambda/c)}{\partial q}_{|q=q_\ell} \Big(- P_1^1(p)\,\sqrt{q_\ell^2-1}\,\underline{u}_\varphi + P_1(p)\,q_\ell\,\underline{e}_3 \Big)\mathrm{d}\varphi\,\mathrm{d}p \end{aligned} \tag{8}$$

where still $\lambda = \ell + 1$ if the interface is included in the average and $\lambda = \ell$ if it is not. Here the choice of λ for the internal or external layer has an influence on the average only in the HC case involving normal flux discontinuities. Otherwise, in the P and LC cases, this choice is only a matter of convenience related to the use of either one or the other set of coefficients. In a similar way as the temperature gradient, (8) can considerably be simplified into a reduced set of terms thanks to the orthogonality of Legendre functions (B.1f). Indeed inserting (3) in (8) yields

$$-\frac{<\underline{u}>_{\mathcal{E}_\ell}}{k_\lambda} = -\Big(a_{\lambda,1}^1 + b_{\lambda,1}^1\,\mathcal{U}_t(q_\ell)\Big)\,\underline{e}_1 - \Big(c_{\lambda,1}^1 + d_{\lambda,1}^1\,\mathcal{U}_t(q_\ell)\Big)\,\underline{e}_2 + \Big(a_{\lambda,1}^0 + b_{\lambda,1}^0\,\mathcal{U}_a(q_\ell)\Big)\,\underline{e}_3 \tag{9}$$

with

$$\mathcal{U}_t(q) = \frac{\sqrt{q^2-1}}{q}\,Q_1^{1'}(q) = \operatorname{arccoth} q + \frac{2-q^2}{q\,(q^2-1)} \quad ; \quad \mathcal{U}_a(q) = Q_1'(q) = \operatorname{arccoth} q - \frac{q}{q^2-1} \tag{10}$$

It finally appears in (6) and (9) that the axial parts (along $\underline{e}_3$) of the averages involve only the first coefficients of order $m = 0$ and the transverse parts involve only the first coefficients of order $m = 1$. Moreover it is of particular interest to notice that the remote boundary condition (1f), in which the position vector is rewritten in terms of spheroidal harmonics (A.3), is obviously also consistent with the order $m = 0$ in the axial direction and $m = 1$ in the transverse one:

$$T \underset{\|\underline{x}\|\to\infty}{\sim} \underline{H}\cdot\underline{x} = -H_1\,c\,P_1^1(p)\,P_1^1(q)\,\cos\varphi - H_2\,c\,P_1^1(p)\,P_1^1(q)\,\sin\varphi + H_3\,c\,P_1(p)\,P_1(q) \tag{11}$$

This remote expression of the temperature field and the symmetries of the problem incite to decompose the problem into a first one corresponding to an axial load ($\underline{H}$ along $\underline{e}_3$) and a second one corresponding to a transverse load ($\underline{H}$ orthogonal to $\underline{e}_3$). By symmetry of revolution of the geometry, the solution of the second problem for an arbitrary $\underline{H}$ orthogonal to $\underline{e}_3$ can be deduced by rotation of the solution obtained for $\underline{H}$ colinear to $\underline{e}_1$.

The resolution detailed in the next section is inspired by the one developed for a N-layer sphere by [5] and [16] in the elastic case and by [13] in the conduction case. However the present problem differs from the latter references by the fact that the non spherical geometry of the inhomogeneity forces to keep infinite sums of harmonics in presence of imperfect interfaces.

2.2. Resolution of the axial problem

In this section, $\underline{H}$ is chosen colinear to $\underline{e}_3$ i.e. $\underline{H} = H_3\,\underline{e}_3$ and $H_1 = H_2 = 0$ in (11). Considering the form of the remote boundary condition and the relationships between the expressions of adjacent layers (1c), (1d) or (1e) involving (3) and (4), it follows that only the terms of order $m = 0$ are kept in the decomposition in each layer. Furthermore the antisymmetry of the problem with respect to the equatorial plane ($p = 0$) implies that the solution should be odd with respect to p so that only the terms of odd degree of the decomposition are non zero:

$$\begin{cases} T_\ell = c \displaystyle\sum_{i=1,3,5\ldots}^{+\infty} P_i(p)\Big(a_{\ell,i}^0\,P_i(q) + b_{\ell,i}^0\,Q_i(q)\Big) & \text{(12a)} \\ \underline{u}_\ell\cdot\underline{e}_q = -\dfrac{k_\ell\,\sqrt{q^2-1}}{\sqrt{q^2-p^2}} \displaystyle\sum_{i=1,3,5\ldots}^{+\infty} P_i(p)\Big(a_{\ell,i}^0\,P_i'(q) + b_{\ell,i}^0\,Q_i'(q)\Big) & \text{(12b)} \end{cases}$$

The solution is fully determined by the knowledge of the sequences $\left(a^0_{\ell,2n-1}\right)_{n\in\mathbb{N}^*}$ and $\left(b^0_{\ell,2n-1}\right)_{n\in\mathbb{N}^*}$ for each layer ℓ ($1 \leq \ell \leq N+1$). These sequences must comply with the remote boundary condition, additional conditions prevailing in the core layer ($\ell = 1$) and interface conditions. The remote boundary condition (11) with $\underline{H} = H_3\,\underline{e}_3$ implies here

$$a^0_{N+1,1} = H_3 \quad \text{and} \quad a^0_{N+1,i} = 0,\ \forall i\ (\text{odd})\ \geq 3 \tag{13}$$

The terms involving the Legendre polynomials of the second kind $Q_i(q)$ become singular in the vicinity of the center of the spheroid, i.e. for the limit $q \to 1$. Consequently the following conditions must be satisfied in the core layer ($\ell = 1$)

$$b^0_{1,i} = 0,\ \forall i\ (\text{odd})\ \geq 0 \tag{14}$$

The determination of the two sets of sequences is finally achieved by invoking the interface conditions (1c), (1d) or (1e) on $\mathcal{I}_\ell$ ($1 \leq \ell \leq N$) in order to relate the sequences of consecutives layers. The interface conditions are expressed as equalities between the infinite series (12a) and (12b) of layers ℓ and $\ell+1$ depending on p (fields are independent of φ in the axial problem) at a given $q = q_\ell$. The case of an interface of P type is rather simple since the continuity of temperature and heat flux through the interface does not mix the two decompositions (12a) and (12b) and thus both conditions involve the same basis of functions of φ and p. It follows that the coefficient of each basis function of p can be identified from the temperature continuity

$$a^0_{\ell+1,i}\,P_i(q_\ell) + b^0_{\ell+1,i}\,Q_i(q_\ell) = a^0_{\ell,i}\,P_i(q_\ell) + b^0_{\ell,i}\,Q_i(q_\ell) \quad \forall i\ (\text{odd})\ \geq 0 \tag{15}$$

and the heat flux continuity

$$k_{\ell+1}\left(a^0_{\ell+1,i}\,P'_i(q_\ell) + b^0_{\ell+1,i}\,Q'_i(q_\ell)\right) = k_\ell\left(a^0_{\ell,i}\,P'_i(q_\ell) + b^0_{\ell,i}\,Q'_i(q_\ell)\right) \quad \forall i\ (\text{odd})\ \geq 0 \tag{16}$$

Conversely the other types of interface LC or HC introduce a mix between temperature and heat flux in one among the two relationships so that the contributions of each basis function of p cannot be uncoupled anymore due to the presence of p in the term before the sum in (12b). As presented in [42], the solution consists in writing the interface condition as a sum in which the terms stemming from the presence of the imperfect interface are written with the coefficients of the internal layer ℓ and then taking the scalar product (as an integral over p) with the i^{th} (i odd) Legendre polynomial. Such a scalar product takes advantage of the orthogonality condition (B.1f) to isolate the coefficients of the $(\ell+1)^{\text{th}}$ layer. As regards the interface of LC type (1d), the continuity of the heat flux (16) still holds whereas (15) is replaced by

$$\begin{aligned} &a^0_{\ell+1,i}\,P_i(q_\ell) + b^0_{\ell+1,i}\,Q_i(q_\ell) = a^0_{\ell,i}\,P_i(q_\ell) + b^0_{\ell,i}\,Q_i(q_\ell) \\ &+\frac{2i+1}{2}\,\frac{k_\ell\,\alpha_\ell}{c}\,\sqrt{q_\ell^2-1}\sum_{j=1,3,5\ldots}^{+\infty} I_{ij}(q_\ell)\left(a^0_{\ell,j}\,P'_j(q_\ell) + b^0_{\ell,j}\,Q'_j(q_\ell)\right) \quad \forall i\ (\text{odd})\ \geq 0 \end{aligned} \tag{17}$$

where I_{ij} is given in (B.7). Note that the practical calculation as provided in AppendixB raises the issue of the numerical accuracy and even convergence of the algorithm. This point is particularly addressed in AppendixC.

The same kind of reasoning can be applied to the HC type interface (1e) at which the temperature field is continuous, which corresponds to (15), and the heat flux discontinuity linearly depends on the surface Laplacian of the temperature. Exploiting (A.11) and the decompositions (12a) and (12b), the second equation of (1e) provides the relationships replacing (16)

$$\begin{aligned} &k_{\ell+1}\left(a^0_{\ell+1,i}\,P'_i(q_\ell) + b^0_{\ell+1,i}\,Q'_i(q_\ell)\right) = k_\ell\left(a^0_{\ell,i}\,P'_i(q_\ell) + b^0_{\ell,i}\,Q'_i(q_\ell)\right) \\ &+\frac{2i+1}{2}\,\frac{\beta_\ell}{c}\,\frac{1}{\sqrt{q_\ell^2-1}}\sum_{j=1,3,5\ldots}^{+\infty} J_{ij}(q_\ell)\left(a^0_{\ell,j}\,P_j(q_\ell) + b^0_{\ell,j}\,Q_j(q_\ell)\right) \quad \forall i\ (\text{odd})\ \geq 0 \end{aligned} \tag{18}$$

where J_{ij} is given in (B.9).

The relationships (17) and (18) involve infinite sums, which are not suitable for a practical numerical implementation. It is then necessary to consider a truncation of the series. The notion of truncation of infinite series of spheroidal harmonics has already been invoked in previous studies ([44], [24]) in which the determination of the optimal threshold was guided by a given tolerance in the variation of coefficients between two successive values of the number of remaining terms. Nevertheless another problem which is evoked above arises here: the calculation of the coupling coefficients I_{ij} and J_{ij} may suffer from a lack of accuracy or even a lack of convergence due to numerical precision as treated in AppendixC. Let $\mathcal{N}$ denote the number of significant terms which are kept in the series (12a) and (12b). As only odd degrees are concerned, this means that the highest degree is $2\mathcal{N}-1$ and the precision is chosen consistently with AppendixC: in other words the precision is taken as the maximum value between $0.8\times(2\mathcal{N}-1)$ and the double precision (16 digits). Let also A^0_ℓ and B^0_ℓ denote the vectors containing the corresponding $\mathcal{N}$ coefficients of layer ℓ and X^0_ℓ their concatenation

$$A^0_\ell=\begin{bmatrix} a^0_{\ell,1}\\ a^0_{\ell,3}\\ \vdots\\ a^0_{\ell,2\mathcal{N}-1}\end{bmatrix}\quad;\quad B^0_\ell=\begin{bmatrix} b^0_{\ell,1}\\ b^0_{\ell,3}\\ \vdots\\ b^0_{\ell,2\mathcal{N}-1}\end{bmatrix}\quad;\quad X^0_\ell=\left[\begin{array}{c} A^0_\ell\\ \hline B^0_\ell\end{array}\right]=\begin{bmatrix} a^0_{\ell,1}\\ \vdots\\ b^0_{\ell,2\mathcal{N}-1}\end{bmatrix} \tag{19}$$

The $(N+1)$ vectors X^0_ℓ contain each $2\mathcal{N}$ components. The resolution of the problem consists then in the identification of these $2\mathcal{N}(N+1)$ variables by means of as many equations. The conditions (13) and (14) can first be written

$$A^0_{N+1}=\begin{bmatrix} H_3\\ 0\\ \vdots\\ 0\end{bmatrix}\quad;\quad B^0_1=\begin{bmatrix} 0\\ 0\\ \vdots\\ 0\end{bmatrix} \tag{20}$$

and the N interface conditions provide $2\mathcal{N}$ more equations. For a perfect interface the linear system gathering the sets of equations (15) and (16) write as

$$\mathcal{J}(k_{\ell+1},q_\ell)X^0_{\ell+1}=\mathcal{J}(k_\ell,q_\ell)X^0_\ell\quad(\mathcal{I}_\ell\text{ of P type}) \tag{21}$$

with the $2\mathcal{N}\times 2\mathcal{N}$ block matrix

$$\mathcal{J}(k,q)=\left[\begin{array}{c|c} \mathcal{J}_P(q) & \mathcal{J}_Q(q)\\ \hline k\mathcal{J}_{P'}(q) & k\mathcal{J}_{Q'}(q)\end{array}\right] \tag{22}$$

in which $\mathcal{J}_P(q)$, $\mathcal{J}_Q(q)$, $\mathcal{J}_{P'}(q)$ and $\mathcal{J}_{Q'}(q)$ are $\mathcal{N}\times\mathcal{N}$ diagonal square matrices generically defined as

$$\mathcal{J}_\mathcal{R}(q)=\begin{bmatrix} \mathcal{R}_1(q) & 0 & \dots & 0\\ 0 & \mathcal{R}_3(q) & \ddots & \vdots\\ \vdots & \ddots & \ddots & 0\\ 0 & \dots & 0 & \mathcal{R}_{2\mathcal{N}-1}(q)\end{bmatrix}\quad\text{with}\quad \mathcal{R}\equiv P,Q,P',Q' \tag{23}$$

As regards the LC interface, the replacement of (15) by (17) induces a change in the right hand side of (21) and more particularly in the upper part of the matrix. Indeed (21) becomes

$$\mathcal{J}(k_{\ell+1},q_\ell)X^0_{\ell+1} = \Big(\mathcal{J}(k_\ell,q_\ell) + \delta\mathcal{J}^{LC}(k_\ell,\alpha_\ell,q_\ell)\Big)X^0_\ell \quad (\mathcal{I}_\ell \text{ of LC type}) \tag{24}$$

with the $2\mathcal{N}\times 2\mathcal{N}$ block matrix

$$\delta\mathcal{J}^{LC}(k,\alpha,q) = \left[\begin{array}{c|c} \delta\mathcal{J}^{LC}_P(k,\alpha,q) & \delta\mathcal{J}^{LC}_Q(k,\alpha,q) \\ \hline [0] & [0] \end{array}\right] \tag{25}$$

in which $\delta\mathcal{J}^{LC}_P(k,\alpha,q)$ and $\delta\mathcal{J}^{LC}_Q(k,\alpha,q)$ are full $\mathcal{N}\times\mathcal{N}$ matrices of generic terms

$$[\delta\mathcal{J}^{LC}_{\mathcal{R}}(k,\alpha,q)]_{rs} = \frac{4r-1}{2}\,\frac{k\,\alpha}{c}\,\sqrt{q^2-1}\,I_{2r-1,2s-1}(q)\,\mathcal{R}'_{2s-1}(q) \quad (1\le r,s\le\mathcal{N}),\ \mathcal{R}\equiv P,Q \tag{26}$$

Simarly for the HC interface, (18) implies that (21) becomes

$$\mathcal{J}(k_{\ell+1},q_\ell)X^0_{\ell+1} = \Big(\mathcal{J}(k_\ell,q_\ell) + \delta\mathcal{J}^{HC}(\beta_\ell,q_\ell)\Big)X^0_\ell \quad (\mathcal{I}_\ell \text{ of HC type}) \tag{27}$$

with the $2\mathcal{N}\times 2\mathcal{N}$ block matrix

$$\delta\mathcal{J}^{HC}(\beta,q) = \left[\begin{array}{c|c} [0] & [0] \\ \hline \delta\mathcal{J}^{HC}_P(\beta,q) & \delta\mathcal{J}^{HC}_Q(\beta,q) \end{array}\right] \tag{28}$$

in which $\delta\mathcal{J}^{HC}_P(\beta,q)$ and $\delta\mathcal{J}^{HC}_Q(\beta,q)$ are full $\mathcal{N}\times\mathcal{N}$ matrices of generic terms

$$[\delta\mathcal{J}^{HC}_{\mathcal{R}}(\beta,q)]_{rs} = \frac{4r-1}{2}\,\frac{\beta}{c}\,\frac{1}{\sqrt{q^2-1}}\,J_{2r-1,2s-1}(q)\,\mathcal{R}_{2s-1}(q) \quad (1\le r,s\le\mathcal{N}),\ \mathcal{R}\equiv P,Q \tag{29}$$

Whatever the type of interface P, LC or HC, the system of equations (21), (24) or (27) always linearly relates the coefficients of layer $\ell+1$ ($X^0_{\ell+1}$) to those of layer ℓ (X^0_ℓ). Indeed multiplying any of these equations by the inverse matrix $\mathcal{J}(k_{\ell+1},q_\ell)^{-1}$ finally yields a system of the form

$$X^0_{\ell+1} = R_\ell X^0_\ell \text{ where } \left\{\begin{array}{ll} R_\ell = \mathcal{J}(k_{\ell+1},q_\ell)^{-1}\mathcal{J}(k_\ell,q_\ell) & \text{(P type)} \\ R_\ell = \mathcal{J}(k_{\ell+1},q_\ell)^{-1}\Big(\mathcal{J}(k_\ell,q_\ell) + \delta\mathcal{J}^{LC}(k_\ell,\alpha_\ell,q_\ell)\Big) & \text{(LC type)} \\ R_\ell = \mathcal{J}(k_{\ell+1},q_\ell)^{-1}\Big(\mathcal{J}(k_\ell,q_\ell) + \delta\mathcal{J}^{HC}(\beta_\ell,q_\ell)\Big) & \text{(HC type)} \end{array}\right. \tag{30}$$

and eventually

$$X^0_{\ell+1} = S_\ell X^0_1 \quad (1\le\ell\le N) \quad \text{with} \quad S_\ell = \prod_{\lambda=1}^{\ell} R_\lambda \tag{31}$$

The coefficients of any layer can then be evaluated from those of the core layer. However the boundary conditions (20) give information on only B^0_1, i.e. the lower half of X^0_1, whereas A^0_1 has first to be determined from A^0_{N+1}. Indeed, decomposing the $2\mathcal{N}\times 2\mathcal{N}$ matrix S_ℓ in four $\mathcal{N}\times\mathcal{N}$ block matrices

$$S_\ell = \left[\begin{array}{c|c} S^{11}_\ell & S^{12}_\ell \\ \hline S^{21}_\ell & S^{22}_\ell \end{array}\right] \tag{32}$$

allows to exploit that $B^0_1 = [0]$ so that $A^0_{N+1} = S^{11}_N A^0_1$ and finally achieves the determination of all the coefficients

$$X^0_{\ell+1} = \begin{bmatrix} A^0_{\ell+1} \\ \hline B^0_{\ell+1} \end{bmatrix} = S_\ell \begin{bmatrix} (S^{11}_N)^{-1} A^0_{N+1} \\ \hline [0] \end{bmatrix} \quad \text{or} \quad \begin{cases} A^0_{\ell+1} = S^{11}_\ell (S^{11}_N)^{-1} A^0_{N+1} \\ B^0_{\ell+1} = S^{21}_\ell (S^{11}_N)^{-1} A^0_{N+1} \end{cases} \tag{33}$$

where A^0_{N+1} is given by (20). In particular, the ratio $b^0_{N+1,1}/a^0_{N+1,1}$, which plays an important role in the implementation of homogenization schemes as shown hereafter, is now readily obtained

$$\frac{b^0_{N+1,1}}{a^0_{N+1,1}} = \sum_{r=1}^{\mathcal{N}} [S^{21}_N]_{1,r} [(S^{11}_N)^{-1}]_{r,1} \tag{34}$$

Indeed these schemes require to calculate the averages of the temperature gradient and the heat flux vector over the whole N-layer spheroid including the external interface. These averages write thanks to (6), (9) and (20)

$$< \underline{h} >_{\mathcal{E}_N} = \left(1 + \frac{b^0_{N+1,1}}{a^0_{N+1,1}} \mathcal{T}_a(q_N) \right) H_3 \, \underline{e}_3 \tag{35}$$

and

$$< \underline{u} >_{\mathcal{E}_N} = -k_{N+1} \left(1 + \frac{b^0_{N+1,1}}{a^0_{N+1,1}} \mathcal{U}_a(q_N) \right) H_3 \, \underline{e}_3 \tag{36}$$

2.3. Resolution of the transverse problem

The resolution of the transverse problem follows the same line as that of the axial one. The macroscopic loading is now of the form (11) with $\underline{H} = H_1 \, \underline{e}_1$ and $H_2 = H_3 = 0$. It comes then that only the terms of order $m = 1$ and proportional to $\cos\varphi$ should be kept here in (3) and (4). Moreover the symmetry with respect to the equatorial plane ($p = 0$) implies that the solution should be even with respect to p. Since the parity of P^1_i is that of $i + 1$, only the terms such that i is odd shall be kept in the decomposition

$$\begin{cases} T_\ell = c \displaystyle\sum_{i=1,3,5\ldots}^{+\infty} P^1_i(p) \left(a^1_{\ell,i} \, P^1_i(q) + b^1_{\ell,i} \, Q^1_i(q) \right) \cos\varphi & \text{(37a)} \\ \underline{u}_\ell \cdot \underline{e}_q = -\dfrac{k_\ell \sqrt{q^2-1}}{\sqrt{q^2-p^2}} \displaystyle\sum_{i=1,3,5\ldots}^{+\infty} P^1_i(p) \left(a^1_{\ell,i} \, P^{1\prime}_i(q) + b^1_{\ell,i} \, Q^{1\prime}_i(q) \right) \cos\varphi & \text{(37b)} \end{cases}$$

Now the sequences to identify are $\left(a^1_{\ell,2n-1}\right)_{n\in\mathbb{N}^*}$ and $\left(b^1_{\ell,2n-1}\right)_{n\in\mathbb{N}^*}$ for each layer ℓ ($1 \le \ell \le N+1$). The remote condition write consistently with (11)

$$a^1_{N+1,1} = -H_1 \quad \text{and} \quad a^1_{N+1,i} = 0, \ \forall i \ (\text{odd}) \ \ge 3 \tag{38}$$

and the singularity in the core implies

$$b^1_{1,i} = 0, \ \forall i \ (\text{odd}) \ \ge 0 \tag{39}$$

The continuity equations characterizing a perfect interface are similar to the axial case: (15) and (16) become here

$$a^1_{\ell+1,i} \, P^1_i(q_\ell) + b^1_{\ell+1,i} \, Q^1_i(q_\ell) = a^1_{\ell,i} \, P^1_i(q_\ell) + b^1_{\ell,i} \, Q^1_i(q_\ell) \quad \forall i \ (\text{odd}) \ \ge 0 \tag{40}$$

and

$$k_{\ell+1} \left(a^1_{\ell+1,i} \, P^{1\prime}_i(q_\ell) + b^1_{\ell+1,i} \, Q^{1\prime}_i(q_\ell) \right) = k_\ell \left(a^1_{\ell,i} \, P^{1\prime}_i(q_\ell) + b^1_{\ell,i} \, Q^{1\prime}_i(q_\ell) \right) \quad \forall i \ (\text{odd}) \ \ge 0 \tag{41}$$

For a LC interface satisfying (1d), (41) remains valid whereas (40) is changed into the counterpart of (17)

$$\begin{aligned} &a^1_{\ell+1,i}\,P^1_i(q_\ell)+b^1_{\ell+1,i}\,Q^1_i(q_\ell)=a^1_{\ell,i}\,P^1_i(q_\ell)+b^1_{\ell,i}\,Q^1_i(q_\ell)\\ &+\frac{2i+1}{2\,i\,(i+1)}\,\frac{k_\ell\,\alpha_\ell}{c}\,\sqrt{q_\ell^2-1}\sum_{j=1,3,5...}^{+\infty}J_{ij}(q_\ell)\Big(a^1_{\ell,j}\,P^{1'}_j(q_\ell)+b^1_{\ell,j}\,Q^{1'}_j(q_\ell)\Big)\quad\forall i\ (\text{odd})\ \geq 0 \end{aligned} \tag{42}$$

where J_{ij} is given in (B.9).

And for a HC interface satisfying (1e), (40) remains valid whereas (41) is changed into the counterpart of (18). After some algebraic calculations making use of (A.11) on (37a) as well as the orthogonality condition (B.1f) to isolate the coefficients of the $(\ell+1)^{\text{th}}$ layer and integration by parts to identify some coupling integrals presented in AppendixB, the heat flux interface equation writes

$$\begin{aligned} &k_{\ell+1}\left(a^1_{\ell+1,i}\,P^{1'}_i(q_\ell)+b^1_{\ell+1,i}\,Q^{1'}_i(q_\ell)\right)=k_\ell\left(a^1_{\ell,i}\,P^{1'}_i(q_\ell)+b^1_{\ell,i}\,Q^{1'}_i(q_\ell)\right)\\ &+\frac{2i+1}{2\,i\,(i+1)}\,\frac{\beta_\ell}{c}\,\frac{1}{\sqrt{q_\ell^2-1}}\sum_{j=1,3,5...}^{+\infty}\left(K_{ij}(q_\ell)+\frac{L_{ij}(q_\ell)}{q_\ell^2-1}\right)\left(a^1_{\ell,j}\,P_j(q_\ell)+b^1_{\ell,j}\,Q_j(q_\ell)\right)\quad\forall i\ (\text{odd})\ \geq 0 \end{aligned} \tag{43}$$

where K_{ij} and L_{ij} are calculated in (B.14) and (B.15).

Still following the reasoning of the axial case, the truncation at non zero $\mathcal{N}$ terms is considered so that the vectors A^1_ℓ, B^1_ℓ and their concatenation X^1_ℓ are introduced similarly as in (19) by replacing the exponent 0 by 1. The conditions (38) and (39) become

$$A^1_{N+1}=\begin{bmatrix}-H_1\\0\\\vdots\\0\end{bmatrix}\quad;\quad B^1_1=\begin{bmatrix}0\\0\\\vdots\\0\end{bmatrix} \tag{44}$$

The transition systems from one layer to its successor still write as (21), (24) or (27) in which the vectors X^0_ℓ and $X^0_{\ell+1}$ are replaced by X^1_ℓ and $X^1_{\ell+1}$, the polynomials in (23) by their corresponding Legendre functions (of the first or second kind) of order $m=1$ (P_n, Q_n, P'_n and Q'_n respectively by P^1_n, Q^1_n, $P^{1'}_n$ and $Q^{1'}_n$) and finally (26) and (29) respectively by

$$[\delta\mathcal{J}^{LC}_{\mathcal{R}}(k,\alpha,q)]_{rs}=\frac{4r-1}{4r(2r-1)}\,\frac{k\,\alpha}{c}\,\sqrt{q^2-1}\,J_{2r-1,2s-1}(q)\,\mathcal{R}^{1'}_{2s-1}(q)\quad(1\leq r,s\leq\mathcal{N}),\ \mathcal{R}\equiv P,Q \tag{45}$$

and

$$[\delta\mathcal{J}^{HC}_{\mathcal{R}}(\beta,q)]_{rs}=\frac{4r-1}{4r(2r-1)}\,\frac{\beta}{c}\,\frac{1}{\sqrt{q^2-1}}\left(K_{2r-1,2s-1}(q)+\frac{L_{2r-1,2s-1}(q)}{q^2-1}\right)\mathcal{R}^1_{2s-1}(q)\quad(1\leq r,s\leq\mathcal{N}),\ \mathcal{R}\equiv P,Q \tag{46}$$

Taking into account these changes in the different matrices, the end of the resolution is similar to the axial case, from the construction of the transition matrices R_ℓ (30) and S_ℓ (31) to the determination of the ratio (34) writing here at the order 1

$$\frac{b^1_{N+1,1}}{a^1_{N+1,1}}=\sum_{r=1}^{\mathcal{N}}[S^{21}_N]_{1,r}[(S^{11}_N)^{-1}]_{r,1} \tag{47}$$

The averages of the temperature gradient and the heat flux vector over the N-layer spheroid including the external interface can be calculated from the first component of (6) and (9). This component differs from the third one corresponding to the axial case not only because of different coefficients and functions but also because of a change of

sign. Nevertheless the final expressions are similar to the axial ones (35) and (36) because this change of sign cancels with the one between $a^0_{N+1,1}$ (13) and $a^1_{N+1,1}$ (38) so that

$$< \underline{h} >_{\mathcal{E}_N} = -\left(1 + \frac{b^1_{N+1,1}}{a^1_{N+1,1}}\,\mathcal{T}_t(q_N)\right) a^1_{N+1,1}\,\underline{e}_1 = \left(1 + \frac{b^1_{N+1,1}}{a^1_{N+1,1}}\,\mathcal{T}_t(q_N)\right) H_1\,\underline{e}_1 \tag{48}$$

and

$$< \underline{u} >_{\mathcal{E}_N} = k_{N+1}\left(1 + \frac{b^1_{N+1,1}}{a^1_{N+1,1}}\,\mathcal{U}_t(q_N)\right) a^1_{N+1,1}\,\underline{e}_1 = -k_{N+1}\left(1 + \frac{b^1_{N+1,1}}{a^1_{N+1,1}}\,\mathcal{U}_t(q_N)\right) H_1\,\underline{e}_1 \tag{49}$$

2.4. Choice of the truncation level

Although the averages (35), (36) (48) and (49) depend only on the first degree coefficients $a^0_{N+1,1}$, $b^0_{N+1,1}$ $a^1_{N+1,1}$ and $b^1_{N+1,1}$ of the matrix, the values of the latter result in general from the complete resolution of both (axial and transversal) systems and consequently vary with the choice of $\mathcal{N}$. In previous works involving infinite series of harmonics (e.g. [24], [35], [25]) the choice of $\mathcal{N}$ has been ruled by a given threshold on the relative difference between the desired quantity calculated for $\mathcal{N}-1$ and that for $\mathcal{N}$. In the present case, the quantities to calculate are $b^0_{N+1,1}/a^0_{N+1,1}$ and $b^1_{N+1,1}/a^1_{N+1,1}$ or actually only $b^0_{N+1,1}$ and $b^1_{N+1,1}$ since $a^0_{N+1,1} = H_3$ and $a^1_{N+1,1} = -H_1$ which can both be set to unit values by linearity. It is worth keeping in mind that, as recalled hereabove and in consistency with AppendixC, the precision of calculation (number of digits) should be chosen in order to ensure the numerical convergence of the interaction integrals I_{ij}, J_{ij}, K_{ij} and L_{ij}, i.e. $\max(0.8 \times (2\mathcal{N}-1), 16)$.

In the case of a single-layer prolate spheroid ($N = 1$) characterized by a resistive core ($k_1 = 0$) and an HC interface of unit normalized surface conductivity ($\beta_1/(b_1 k_2) = 1$ where b_1 denotes the small radius of the prolate spheroid), the relative differences between the values of $b^0_{N+1,1}$ on the one hand and $b^1_{N+1,1}$ on the other hand for $\mathcal{N}-1$ and those for $\mathcal{N}$ are drawn in Figure 2. It appears in this case that only 5 terms are necessary to stay below 10^{-3} and 10 terms to stay below 10^{-4} whatever the aspect ratio. It is worth noticing that the number of 10 terms remains lower than that triggering the need to resort to multiple precision numbers since $0.8 \times (2\mathcal{N}-1)$ is lower than 16 digits but these figures may not hold with other configurations ($N > 1$ and different conductivities…). However, if necessary, a better accuracy may still be obtained thanks to the analysis of convergence in AppendixC.

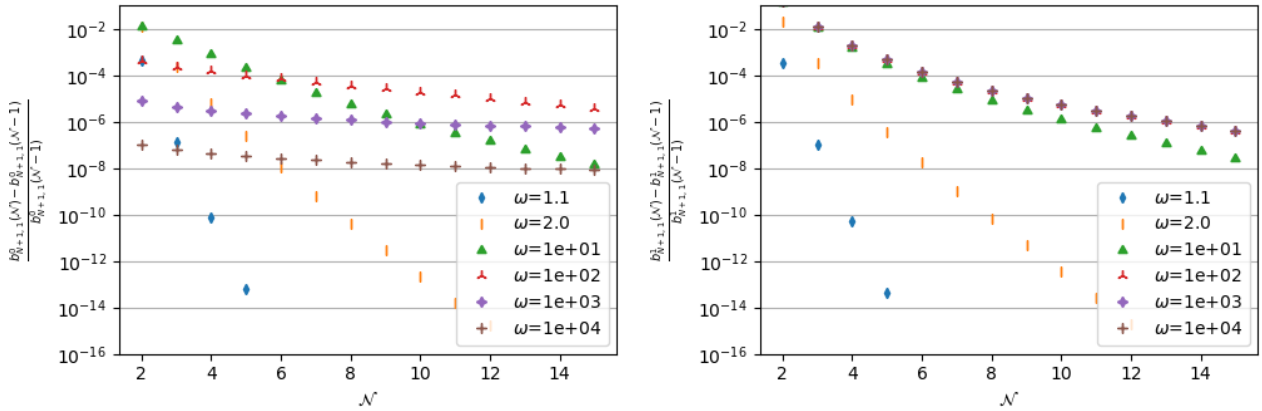

Figure 2: Relative difference between successive estimations of $b^0_{N+1,1}$ and $b^1_{N+1,1}$ in the case of a single-layer prolate spheroid ($N = 1$) with $k_1 = 0$ (resistive core), HC interface $\beta_1/(b_1 k_2) = 1$ (b_1: small radius) and various aspect ratios

3. Particular case of a confocal N-layer spheroid with perfect interfaces only

It has been shown in the previous section that the complete solution of the conduction Eshelby problem of a N-layer confocal spheroid is estimated by resolution of a system of equations corresponding to interface conditions relating the temperature and normal flux expressions of a layer to those of the adjacent layer. In general these expressions write as infinite sums because of the couplings between harmonics of the same order but different degrees arising in the cases of imperfect interface conditions. Indeed the latter introduce a mix between temperature (3) and normal flux (4) which are not decomposed in the same basis of orthogonal functions and which induce equations such as (17), (18), (42) and (43) involving coupling integrals I_{ij}, J_{ij} and K_{ij}. However in the case of a N-layer sphere, it can be shown that the decompositions of the temperature and the normal flux are consistent at a given radius (see for instance equations (7) and (8) of [13]). This means that, even in the case of imperfect interfaces, only two harmonics (one regular and one irregular) and two coefficients per layer are needed. Coming back to the confocal N-layer spheroidal problem, the complete resolution developed in the previous section shows that here again only the first regular and irregular harmonics are involved in the solution if all the interfaces are of perfect type, as presented hereafter.

3.1. Axial problem

As in section 2.2, this problem corresponds to a macroscopic temperature gradient of the form $\underline{H} = H_3\underline{e}_3$. The continuity conditions at the interfaces are expressed in (15) and (16). The latter together with the remote conditions (13) and regularity at the origin (14) imply that the solution writes in each layer ℓ

$$\begin{cases} T_\ell = c\,P_1(p)\left(a_\ell^0\,P_1(q) + b_\ell^0\,Q_1(q)\right) = \left(a_\ell^0 + b_\ell^0\,\mathcal{T}_a(q)\right)\underline{e}_3\cdot\underline{x} & \text{(50a)} \\ \underline{u}_\ell\cdot\underline{e}_q = -k_\ell\,\dfrac{\sqrt{q^2-1}}{\sqrt{q^2-p^2}}\,P_1(p)\left(a_\ell^0\,P_1'(q) + b_\ell^0\,Q_1'(q)\right) = -k_\ell\left(a_\ell^0 + b_\ell^0\,\mathcal{U}_a(q)\right)\underline{e}_3\cdot\underline{e}_q & \text{(50b)} \end{cases}$$

with $\mathcal{T}_a$ and $\mathcal{U}_a$ defined in (7) and (10) and $\underline{x}$ and $\underline{e}_q$ written as in (A.3) and (A.6). The reference to the degree 1 has been omitted in the coefficients, i.e. a_ℓ^0 and b_ℓ^0 instead of $a_{\ell,1}^0$ and $b_{\ell,1}^0$ since only this degree is involved in the solution here while the superscript 0 corresponding to the order is kept to distinguish the axial and the transverse solutions. The consistency with the averages already obtained in the general case in (6) and (9) is straightforward by Stokes theorem. Interestingly here the solution in temperature over any spheroid of linear eccentricity c defined as an iso-q surface has the same structure as the remote condition (1f). Indeed (50a) writes $T_\ell = \lambda(q)\underline{e}_3\cdot\underline{x}$ with $\lambda(q) = a_\ell^0 + b_\ell^0\,\mathcal{T}_a(q)$. It is then possible to consider the problem of conduction posed only on the spheroid $\mathcal{E}_\ell$ with boundary condition of the form $T = \lambda(q_\ell)\underline{e}_3\cdot\underline{x}$ at finite distance over $\mathcal{I}_\ell$. By linearity, there exists a function $k_\ell^{a,eq}$ depending only on the material property and geometrical characteristics of the ℓ-layer spheroid $\mathcal{E}_\ell$ such that $\underline{u}\cdot\underline{e}_q = -k_\ell^{a,eq}\lambda(q_\ell)\underline{e}_3\cdot\underline{e}_q$ over $\mathcal{I}_\ell$. Using Stokes theorem, this also means that $<\underline{u}>_\ell = -k_\ell^{a,eq} <\underline{h}>_{\mathcal{E}_\ell}$ where $k_\ell^{a,eq}$ can be interpreted as the equivalent axial conductivity of the ℓ-layer spheroid $\mathcal{E}_\ell$ and also writes by consistency with (50a) and (50b)

$$k_\ell^{a,eq} = k_\ell\,\frac{a_\ell^0 + b_\ell^0\,\mathcal{U}_a(q_\ell)}{a_\ell^0 + b_\ell^0\,\mathcal{T}_a(q_\ell)} \tag{51}$$

By unicity of the solution it comes that the temperature and flux fields outside $\mathcal{E}_\ell$ remain unchanged if the composite spheroid $\mathcal{E}_\ell$ is replaced by a homogeneous one of axial conductivity equal to $k_\ell^{a,eq}$.

Although theoretically clear from this reasoning based on linearity and on the form of the solution (50a), the fact that $k_\ell^{a,eq}$ does not depend on the layers which are outside $\mathcal{E}_\ell$ may not be obvious in (51) since the coefficients a_ℓ^0 and b_ℓ^0 are built from the complete problem involving the whole system. The equations to be solved stem from (21) with $\mathcal{N} = 1$ without any need to invoke any truncation here since the exact solution only requires $\mathcal{N} = 1$. In the current framework, (21) alternatively writes

$$\begin{cases} a_{\ell+1}^0 + b_{\ell+1}^0\,\mathcal{T}_a(q_\ell) = a_\ell^0 + b_\ell^0\,\mathcal{T}_a(q_\ell) & \text{(52a)} \\ k_{\ell+1}\left(a_{\ell+1}^0 + b_{\ell+1}^0\,\mathcal{U}_a(q_\ell)\right) = k_\ell\left(a_\ell^0 + b_\ell^0\,\mathcal{U}_a(q_\ell)\right) & \text{(52b)} \end{cases}$$

Furthermore (20) recalls that the core layer depends on one single scalar coefficient a_1^0 which can eventually be related to the remote temperature gradient $a_{N+1}^0 = H_3$ by $a_1^0 = H_3/S_N^{11}$ since S_N^{11} in (32) is scalar here. Finally from (31) the coefficients of layer $\ell > 1$ are deduced from the single one of the core layer by simple linear relationships $a_\ell^0 = S_{\ell-1}^{11} a_1^0$ and $b_\ell^0 = S_{\ell-1}^{21} a_1^0$ where the scalars $S_{\ell-1}^{11}$ and $S_{\ell-1}^{21}$ only depend by construction on the material and geometrical characteristics of the spheroid $\mathcal{E}_\ell$ bounded by $\mathcal{I}_\ell$. It follows from (50a) and (50b) that

$$\begin{cases} T_\ell = a_1^0 \left(S_{\ell-1}^{11} + S_{\ell-1}^{21} \mathcal{T}_a(q) \right) \underline{e}_3 \cdot \underline{x} & \text{(53a)} \\ \underline{u}_\ell \cdot \underline{e}_q = -a_1^0 k_\ell \left(S_{\ell-1}^{11} + S_{\ell-1}^{21} \mathcal{U}_a(q) \right) \underline{e}_3 \cdot \underline{e}_q & \text{(53b)} \end{cases}$$

It also results that the equivalent conductivity of the ℓ-layer spheroid $\mathcal{E}_\ell$ rewrites

$$k_\ell^{a,eq} = k_\ell \frac{S_{\ell-1}^{11} + S_{\ell-1}^{21} \mathcal{U}_a(q_\ell)}{S_{\ell-1}^{11} + S_{\ell-1}^{21} \mathcal{T}_a(q_\ell)} \tag{54}$$

which confirms that $k_\ell^{a,eq}$ depends only on the internal characteristics of $\mathcal{E}_\ell$.

Besides the general solution provided in the last section, it is now interesting to examine more in details how to express practically the solution (50a) and (50b) and the values $k_\ell^{a,eq}$ in the light of this notion of equivalent of sub-spheroid, through a recursive procedure.

Case $N = 1$

This case corresponds to a uniform spheroid embedded in an infinite matrix, in other words to the classical Eshelby problem. The unknowns a_1^0 and b_2^0 are determined by the system (52a)-(52b) in which $\ell = 1$ and $a_2^0 = H_3$ and $b_1^0 = 0$

$$\begin{cases} a_1^0 = \left(1 + \dfrac{k_1 - k_2}{k_2} \dfrac{\mathcal{T}_a(q_1)}{\mathcal{T}_a(q_1) - \mathcal{U}_a(q_1)} \right)^{-1} a_2^0 & \text{(55a)} \\ b_2^0 = \dfrac{k_2 - k_1}{k_1 \mathcal{T}_a(q_1) - k_2 \mathcal{U}_a(q_1)} a_2^0 & \text{(55b)} \end{cases}$$

As expected, the expression (55a) relating the uniform axial temperature gradient to the remote one exactly corresponds to the axial component of the Eshelby solution as recalled in AppendixD ([1], [45]). Indeed the axial component of the Eshelby tensor can be retrieved from (55a) by exploiting (7) and (10) as well as (A.4)

$$S_a(q) = \frac{\mathcal{T}_a(q)}{\mathcal{T}_a(q) - \mathcal{U}_a(q)} = \left(q^2 - 1 \right) (q \ \mathrm{arccoth}\, q - 1) \quad \text{with } q = \frac{\omega}{\sqrt{\omega^2 - 1}} \tag{56}$$

which boils down to the axial component of the prolate case ($\omega > 1$) of (D.3). It is worth recalling here that this results also holds for the oblate case ($\omega < 1$) after applying the formal transformation $q = \imath\tau$ introduced in AppendixA and (A.5)

$$S_a(\imath\tau) = \left(1 + \tau^2 \right) (1 - \tau \ \mathrm{arccot}\, \tau) \quad \text{with } \tau = \frac{\omega}{\sqrt{1 - \omega^2}} \tag{57}$$

Case $N = 2$

As recalled hereabove in (51) and associated comments, the two-layer spheroid $\mathcal{E}_2$ can be replaced by a homogeneous spheroid of axial conductivity

$$k_2^{a,eq} = k_\ell \frac{a_2^0 + b_2^0 \mathcal{U}_a(q_2)}{a_2^0 + b_2^0 \mathcal{T}_a(q_2)} \tag{58}$$

without disturbing the solution established in the matrix Ω_3. Moreover the relationships (55a) and (55b) remain valid since they only come from the continuity equations on $\mathcal{I}_1$ and $b_1^0 = 0$. Introducing then b_2^0 (55b) into (58), the latter becomes after some algebra

$$k_2^{a,eq} = k_2 + \frac{\mathcal{T}_a(q_2) - \mathcal{U}_a(q_2)}{\mathcal{T}_a(q_1) - \mathcal{U}_a(q_1)} \left(\frac{1}{k_1 - k_2} + \frac{1}{k_2} \frac{\mathcal{T}_a(q_1) - \mathcal{T}_a(q_2)}{\mathcal{T}_a(q_1) - \mathcal{U}_a(q_1)} \right)^{-1} \tag{59}$$

The definitions (7) and (10) can again be exploited to rewrite (59). It is worth noting first that

$$f_1 = \frac{\mathcal{T}_a(q_2) - \mathcal{U}_a(q_2)}{\mathcal{T}_a(q_1) - \mathcal{U}_a(q_1)} = \frac{q_1\left(q_1^2 - 1\right)}{q_2\left(q_2^2 - 1\right)} \tag{60}$$

corresponds to the volume fraction occupied by the core $\mathcal{E}_1$ within $\mathcal{E}_2$. Then from (56), the relationships are obtained

$$S_a(q_1) = \frac{\mathcal{T}_a(q_1)}{\mathcal{T}_a(q_1) - \mathcal{U}_a(q_1)} \quad ; \quad f_1\, S_a(q_2) = \frac{\mathcal{T}_a(q_2)}{\mathcal{T}_a(q_1) - \mathcal{U}_a(q_1)} \tag{61}$$

so that (59) becomes

$$k_2^{a,eq} = k_2 + f_1\left(\frac{1}{k_1 - k_2} + \frac{S_a(q_1) - f_1\, S_a(q_2)}{k_2}\right)^{-1} \tag{62}$$

where once again the replacement of q by $\imath\tau$ allows to consider oblate instead of prolate spheroids.

Recursive procedure to the general case N

The solution to the N-layer spheroidal inhomogeneity can be obtained by analogy with the two-layer one using a recursive homogenization strategy consisting in building step-by-step from $\ell = 1$ to $\ell = N$ the equivalent homogeneous spheroid comprising the ℓ first layers starting from the core (see figure 3). Namely, for a given $1 \leq \ell \leq N-1$, the ℓ first internal layers are replaced by an equivalent spheroid and the composite two-layer spheroid made up with this equivalent core surrounded by the $(\ell+1)^{\text{th}}$ layer is finally considered. The strategy employed with the two-layer case together with the reasoning showing that the field outside the internal spheroid is not perturbed by the replacement of the latter by an equivalent homogeneous core leads to the following adaptation of (62)

$$k_{\ell+1}^{a,eq} = k_{\ell+1} + f_\ell\left(\frac{1}{k_\ell^{a,eq} - k_{\ell+1}} + \frac{S_a(q_\ell) - f_\ell\, S_a(q_{\ell+1})}{k_{\ell+1}}\right)^{-1} \text{ with } f_\ell = \frac{|\mathcal{E}_\ell|}{|\mathcal{E}_{\ell+1}|} = \frac{q_\ell\left(q_\ell^2 - 1\right)}{q_{\ell+1}\left(q_{\ell+1}^2 - 1\right)} \tag{63}$$

Once the successive values of $k_\ell^{a,eq}$ have been identified starting from $k_1^{a,eq} = k_1$ to finish with $k_N^{a,eq}$ corresponding to

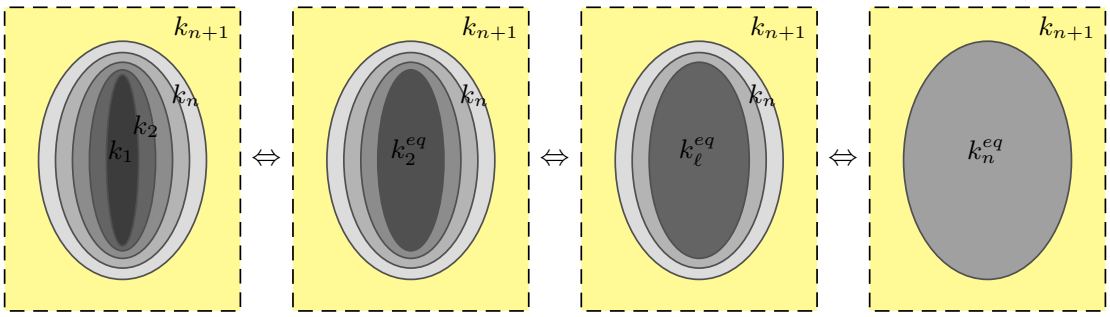

Figure 3: Recursive procedure for the equivalent conductivity

the whole composite equivalent axial conductivity, it may be convenient to notice that a recursive procedure can also be used, alternatively to the general strategy developed in section 2, to identify all the coefficients a_ℓ^0 and b_ℓ^0 giving the complete solution fields. This recursive procedure starts from the outside to reach, layer by layer, the core of the spheroid. The outside constants are determined by the remote condition on the one hand and the analogy with (55b) on the other hand considering the equivalent spheroid instead of the N-layer composite

$$a_{N+1}^0 = H_3 \quad ; \quad b_{N+1}^0 = \frac{k_{N+1} - k_N^{a,eq}}{k_N^{a,eq}\,\mathcal{T}_a(q_N) - k_{N+1}\,\mathcal{U}_a(q_N)}\, H_3 \tag{64}$$

Then assuming that the constants of layer $\ell+1$ are known, those of layer ℓ are obtained through a reasoning based first on the introduction of the average axial temperature gradient in $\mathcal{E}_\ell$ identified in (6) as $a'_\ell = a^0_\ell + b^0_\ell \mathcal{T}_a(q_\ell)$. Exploiting then the definition of $k^{a,eq}_\ell$ in (51), the system (52a)-(52b) writes

$$\begin{cases} a^0_{\ell+1} + b^0_{\ell+1}\,\mathcal{T}_a(q_\ell) = a'_\ell & \text{(65a)} \\ k_{\ell+1}\left(a^0_{\ell+1} + b^0_{\ell+1}\,\mathcal{U}_a(q_\ell)\right) = k^{a,eq}_\ell\, a'_\ell & \text{(65b)} \end{cases}$$

This system is formally analogous to that of the single spheroid case in which the constant corresponding to the irregular harmonics vanishes, leading then to the solution (55a)

$$a'_\ell = \left(1 + \frac{k^{a,eq}_\ell - k_{\ell+1}}{k_{\ell+1}} \frac{\mathcal{T}_a(q_\ell)}{\mathcal{T}_a(q_\ell) - \mathcal{U}_a(q_\ell)}\right)^{-1} a^0_{\ell+1} \tag{66}$$

The end of the identification is finally achieved by solving the system made by $a'_\ell = a^0_\ell + b^0_\ell \mathcal{T}_a(q_\ell)$ and (51)

$$\begin{cases} a^0_\ell = \dfrac{k^{a,eq}_\ell \mathcal{T}_a(q_\ell) - k_\ell \mathcal{U}_a(q_\ell)}{k_\ell\left(\mathcal{T}_a(q_\ell) - \mathcal{U}_a(q_\ell)\right)} a'_\ell & \text{(67a)} \\ b^0_\ell = \dfrac{k_\ell - k^{a,eq}_\ell}{k_\ell\left(\mathcal{T}_a(q_\ell) - \mathcal{U}_a(q_\ell)\right)} a'_\ell & \text{(67b)} \end{cases}$$

3.2. Transverse problem

This section is analogous to 3.1 with a remote temperature gradient here equal to $\underline{H} = H_1 \underline{e}_1$, which means that the solutions (50a) and (50b) now become

$$\begin{cases} T_\ell = c\, P^1_1(p)\left(a^1_\ell\, P^1_1(q) + b^1_\ell\, Q^1_1(q)\right)\cos\varphi = -\left(a^1_\ell + b^1_\ell\,\mathcal{T}_t(q)\right)\underline{e}_1 \cdot \underline{x} & \text{(68a)} \\ \underline{u}_\ell \cdot \underline{e}_q = -k_\ell \dfrac{\sqrt{q^2-1}}{\sqrt{q^2-p^2}} P^1_1(p)\left(a^1_\ell\, P^{1'}_1(q) + b^1_\ell\, Q^{1'}_1(q)\right)\cos\varphi = k_\ell\left(a^1_\ell + b^1_\ell\,\mathcal{U}_t(q)\right)\underline{e}_1 \cdot \underline{e}_q & \text{(68b)} \end{cases}$$

with $\mathcal{T}_t$ and $\mathcal{U}_t$ defined in (7) and (10) and $\underline{x}$ and $\underline{e}_q$ written as in (A.3) and (A.6). It makes no doubt that all the reasoning and developments of the axial problem can be reproduced here only changing H_3 by H_1, the coefficients a^0_ℓ and b^0_ℓ by $-a^1_\ell$ and $-b^1_\ell$ and the functions $\mathcal{T}_a$ and $\mathcal{U}_a$ by $\mathcal{T}_t$ and $\mathcal{U}_t$. In particular, the transverse component of the Eshelby tensor can be identified by analogy with (56)

$$S_t(q) = \frac{\mathcal{T}_t(q)}{\mathcal{T}_t(q) - \mathcal{U}_t(q)} = \frac{q}{2}\left(q - \left(q^2-1\right)\operatorname{arccoth} q\right) \quad \text{with } q = \frac{\omega}{\sqrt{\omega^2-1}} \tag{69}$$

also consistent with the prolate case of (D.3) as well as the oblate case provided that the transformation $q = \imath\tau$ is applied

$$S_t(\imath\tau) = \frac{\tau}{2}\left(\left(1+\tau^2\right)\operatorname{arccot}\tau - \tau\right) \quad \text{with } \tau = \frac{\omega}{\sqrt{1-\omega^2}} \tag{70}$$

Besides the notion of equivalent conductivity depending only on the internal characteristics of the corresponding ellipsoid still holds as defined by the transverse counterpart of (51)

$$k^{t,eq}_\ell = k_\ell \frac{a^1_\ell + b^1_\ell\,\mathcal{U}_t(q_\ell)}{a^1_\ell + b^1_\ell\,\mathcal{T}_t(q_\ell)} \tag{71}$$

and satisfies a recursive definition analogous to (63)

$$k^{t,eq}_{\ell+1} = k_{\ell+1} + f_\ell \left(\frac{1}{k^{t,eq}_\ell - k_{\ell+1}} + \frac{S_t(q_\ell) - f_\ell\, S_t(q_{\ell+1})}{k_{\ell+1}}\right)^{-1} \quad \text{with } k^{t,eq}_1 = k_1 \tag{72}$$

Finally the back recursive strategy leading to (64)-(67b) can also be adapted here to the transverse problem to identify all the coefficients a_ℓ^1 and b_ℓ^1, still changing H_3 by H_1, a_ℓ^0 and b_ℓ^0 by $-a_\ell^1$ and $-b_\ell^1$, $\mathcal{T}_a$ and $\mathcal{U}_a$ by $\mathcal{T}_t$ and $\mathcal{U}_t$ and $k_\ell^{a,eq}$ by $k_\ell^{t,eq}$.

Gathering the component expressions (63) and (72), the equivalent conductivity of the successive spheroids $\mathcal{E}_\ell$ can be written under the following recursive tensor form

$$\boldsymbol{k}_{\ell+1}^{eq} = \boldsymbol{k}_{\ell+1} + f_\ell \left(\left(\boldsymbol{k}_\ell^{eq} - \boldsymbol{k}_{\ell+1} \right)^{-1} + \left(\boldsymbol{S}^{\mathcal{E}}(\omega_\ell) - f_\ell \, \boldsymbol{S}^{\mathcal{E}}(\omega_{\ell+1}) \right) \cdot \boldsymbol{k}_{\ell+1}^{-1} \right)^{-1} \text{ with } \boldsymbol{k}_1^{eq} = \boldsymbol{k}_1 \tag{73}$$

where the generic Eshelby tensor $\boldsymbol{S}^{\mathcal{E}}$ is given as a function of the aspect ratio in (D.2)-(D.3).

3.3. Analogy with the Ponte-Castañeda-Willis bound

This section aims at putting in evidence that the recursive relationship (73) is actually intimately related to the Ponte-Castañeda-Willis (PCW) bound [46] applied to a two-phase matrix composite. In the framework adopted in [46] transposed from elasticity to conductivity, a matrix of conductivity $\boldsymbol{k}_m$ and aligned inhomogeneities of conductivity $\boldsymbol{k}_c$ and volume fraction f are considered. One of the interest of the PCW bound relies upon the uncoupling between the individual shapes and mutual spatial distribution of phases. Here the particle shape as well as the unique spatial distribution are assumed to be ellipsoidal and therefore associated to Eshelby tensors respectively denoted by $\boldsymbol{S}_m^c$ and $\boldsymbol{S}_m^{\mathcal{D}}$ (depending on the matrix $\boldsymbol{k}_m$ only if the latter is anisotropic as recalled in AppendixD). The PCW bound writes from [46]

$$\boldsymbol{k}^{\text{PCW}} = \boldsymbol{k}_m + f \left((\boldsymbol{k}_c - \boldsymbol{k}_m)^{-1} + \left(\boldsymbol{S}_m^c - f \, \boldsymbol{S}_m^{\mathcal{D}} \right) \cdot \boldsymbol{k}_m^{-1} \right)^{-1} \tag{74}$$

Note that the upper or lower status of the bound depends on the contrast between the two phases. This bound can anyway be considered as an estimate. It is also worth recalling that, in this condition of unique spatial distribution, the PCW bound coincides with the Maxwell scheme estimate provided that the shape related to the spatial distribution plays the role of the shape of the effective particle as emphasized in [47]. In the case of spheroidal shapes, isotropy of the matrix and spatial distribution respectively associated to the aspect ratios ω_c and $\omega_{\mathcal{D}}$, the Eshelby tensors in (74) can be calculated by (D.2)-(D.3).

It is clear now that the recursive formula (73) coincides with the formal application of (74) in which the role of the matrix is played by the surrounding material $\boldsymbol{k}_m = \boldsymbol{k}_{\ell+1}$, the role of the particle is played by the effective core $\boldsymbol{k}_c = \boldsymbol{k}_\ell^{eq}$ of volume fraction equal to the ratio between $|\mathcal{E}_\ell|$ and $|\mathcal{E}_{\ell+1}|$ i.e. $f = f_\ell$ and the shape of the particle corresponds to that of the internal core of aspect ratio $\omega_c = \omega_\ell$ whereas the shape of the distribution corresponds to that of the external boundary $\omega_{\mathcal{D}} = \omega_{\ell+1}$.

The correspondence between these two expressions deserves some comments. Indeed the interpretation of the recursive formula in terms of PCW bound somehow casts a new light on the notion of security ellipsoids introduced in [46]. This notion, which is schematized by aligned ellipsoids in Figure 2 of [46], is related to a mathematical concept of spatial distribution in the latter reference whereas it explicitly corresponds to a geometrical definition in the case of the two-layer spheroid leading to (73). On the one hand, the PCW bound of a two-phase composite as presented hereabove is restricted to a single shape and orientation of the spatial distribution but there is no limitation about the choice of this ellipsoidal shape: in particular it is independent of the particle one provided that the volume fraction allows a configuration without overlapping of security ellipsoids. Furthermore, the PCW bound (74) is not restricted to isotropic behavior. On the other hand, the solution to the two-layer spheroid is restricted to confocal spheroids delimiting the surrounding zone which is assumed isotropic whereas the core can be transverse isotropic with the same symmetry axis as the particle. Nevertheless, this solution is obtained in the framework of an auxiliary Eshelby problem, which means that it can be further used in homogenization schemes involving arbitrary directions of several sets of such particles including their security spheroids as drawn in figure 4.

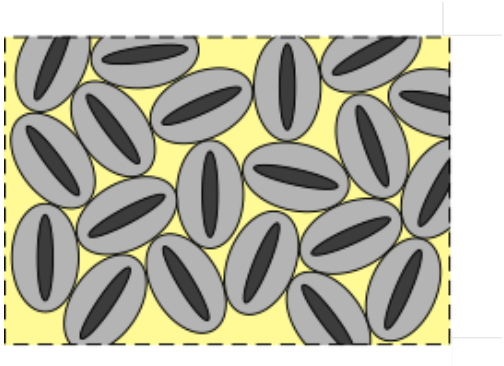

Figure 4: Isotropic distribution of orientation of spheroidal particles surrounded by security spheroids

4. Notion of equivalent particle in conduction

The notion of equivalent particle is now first examined in the framework of the confocal N-layer spheroid for which a complete solution has been derived. Then, after general considerations about ellipsoidal equivalent particles, a particular focus is paid on the case of a homogeneous spheroid with an imperfect interface reviewing some already published results and providing some extensions in a simplified framework.

4.1. Case of the confocal N-layer spheroid

It has been shown in section 3 that a confocal N-layer spheroid with perfect interfaces has actually the same overall interaction with its surrounding material as a homogeneous spheroid of conductivity defined by the recursive algorithm (73). In particular, it has been highlighted in this case that the equivalent conduction only depends on the internal content of the spheroid and not on the surrounding material. This result does not hold anymore in presence of imperfect interfaces. In the latter case, it is however possible to define an equivalent conductivity by taking advantage of (35), (36), (48) and (49)

$$\boldsymbol{k}^{eq} = k_{N+1}\left(\frac{1+\frac{b^1_{N+1,1}}{a^1_{N+1,1}}\mathcal{U}_t(q_N)}{1+\frac{b^1_{N+1,1}}{a^1_{N+1,1}}\mathcal{T}_t(q_N)}\left(\mathbf{1}-\underline{e}_3\otimes\underline{e}_3\right)+\frac{1+\frac{b^0_{N+1,1}}{a^0_{N+1,1}}\mathcal{U}_a(q_N)}{1+\frac{b^0_{N+1,1}}{a^0_{N+1,1}}\mathcal{T}_a(q_N)}\underline{e}_3\otimes\underline{e}_3\right) \tag{75}$$

depending on the ratios $b^0_{N+1,1}/a^0_{N+1,1}$ and $b^1_{N+1,1}/a^1_{N+1,1}$ which have been obtained from (34) and (47). In general, due to the presence of imperfect interfaces inducing infinite series of harmonics in each layer and more particularly in the core, this equivalent conductivity actually depends on the conductivity k_{N+1} of the surrounding material. Nevertheless it may be noted that not only the composite and the equivalent particle have the same overall conductivity (by definition) but they also both have the same temperature gradient and heat flux vector averages over the particle which are the required quantities in homogenization schemes relying on auxiliary Eshelby problems. Indeed these averages within the composite and the equivalent particle have the same structure (35), (36), (48) and (49) also depending on the ratios $b^0_{N+1,1}/a^0_{N+1,1}$ and $b^1_{N+1,1}/a^1_{N+1,1}$ involving coefficients in the infinite matrix. The equality (75) also means the equality between the corresponding ratios of both problems (the ratio of the axial resp. transverse problem of the N-layer spheroid is equal to the ratio of the axial resp. transverse problem of the equivalent spheroid) and consequently the equality between the corresponding averages (35), (36), (48) and (49).

4.2. General definition and construction of concentration tensor averages

The considerations on an equivalent ellipsoid in the particular cases discussed in sections 3.1 and 4.1 are now extended to the general case of an arbitrarily heterogeneous inclusion. An equivalent particle of a composite is defined as a homogeneous particle occupying the same domain and having the same overall interaction effect with

its vicinity. In the framework of an Eshelby problem defined by an infinite matrix of conductivity $\boldsymbol{k}_m$ (or resistivity $\boldsymbol{r}_m = \boldsymbol{k}_m^{-1}$) and an ellipsoidal composite $\mathcal{E}$ subjected to a remote temperature gradient $\underline{H}$, it is possible to introduce concentration tensors $\boldsymbol{A}(\underline{x})$ and $\boldsymbol{B}(\underline{x})$ satisfying (2) whatever the distribution of heterogeneities within $\mathcal{E}$. It follows that the average values of temperature gradient and heat flux vector within $\mathcal{E}$ are related by

$$< \underline{u} >_{\mathcal{E}} = -\boldsymbol{k}^{eq} \cdot < \underline{h} >_{\mathcal{E}} \quad \text{with} \quad \boldsymbol{k}^{eq} = < \boldsymbol{B} >_{\mathcal{E}} \cdot < \boldsymbol{A} >_{\mathcal{E}}^{-1} \quad \text{or} \quad \boldsymbol{r}^{eq} = \boldsymbol{k}^{eq-1} = < \boldsymbol{A} >_{\mathcal{E}} \cdot < \boldsymbol{B} >_{\mathcal{E}}^{-1} \tag{76}$$

which can be considered as a definition of an equivalent thermal conductivity or resistivity (see figure 5). Such a

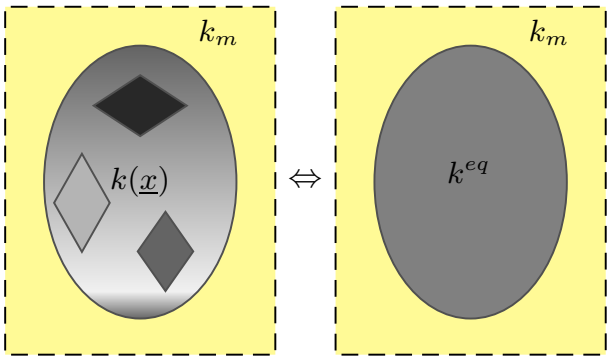

Figure 5: Principle of replacement of a composite particle by an equivalent one

definition (76) may raise the issue of the symmetry $\boldsymbol{k}^{eq}$ or $\boldsymbol{r}^{eq}$ but this important general question will not be addressed in this work since the symmetries of the considered problems in the sequel imply that $< \boldsymbol{A} >_{\mathcal{E}}$ and $< \boldsymbol{B} >_{\mathcal{E}}$ are diagonalized in the same frame, which ensures the symmetry of $\boldsymbol{k}^{eq}$. Besides, unlike very particular cases as that of a confocal N-layer spheroid with perfect interfaces, $\boldsymbol{k}^{eq}$ as expressed in (76) is generally not independent of the property of the reference medium in which the particle is embedded. Such a dependence somehow weakens the intrinsic character of the notion of equivalent particle since the equivalent property of the particle may be sensitive to any change of the matrix behavior. This also raises the issue of the determination of an equivalent particle within a representative volume element in the framework of Eshelby-based homogenization schemes. Indeed the reference medium playing the role of the matrix in the auxiliary Eshelby problem in which the particle is embedded depends on the choice of the scheme (the matrix itself for dilute, Mori-Tanaka or Maxwell schemes and the homogenized medium for the self-consistent scheme), which may introduce different definitions of the equivalent particle. Nevertheless, whether $\boldsymbol{k}^{eq}$ depends or not on $\boldsymbol{k}_m$, it is proven in AppendixF by means of the integral solution, that the average concentration tensors $< \boldsymbol{A} >_{\mathcal{E}}$ and $< \boldsymbol{B} >_{\mathcal{E}}$ which are needed in homogenization schemes are rigorously provided by the Eshelby solution of the equivalent particle (F.4)

$$< \boldsymbol{A} >_{\mathcal{E}} = \left(\boldsymbol{1} + \boldsymbol{S}_m^{\mathcal{E}} \cdot \boldsymbol{k}_m^{-1} \cdot (\boldsymbol{k}^{eq} - \boldsymbol{k}_m)\right)^{-1} \quad ; \quad < \boldsymbol{B} >_{\mathcal{E}} = \boldsymbol{k}^{eq} \cdot \left(\boldsymbol{1} + \boldsymbol{S}_m^{\mathcal{E}} \cdot \boldsymbol{k}_m^{-1} \cdot (\boldsymbol{k}^{eq} - \boldsymbol{k}_m)\right)^{-1} \tag{77}$$

Although intuitively expected, this result was not obvious since only the products $< \boldsymbol{B} >_{\mathcal{E}} \cdot < \boldsymbol{A} >_{\mathcal{E}}^{-1}$ were initially identical in the real and equivalent problems. Note that it holds for any anisotropic behavior of materials, distribution of heterogeneities in the composite particle and external ellipsoidal shape of the latter.

4.3. Case of a homogeneous spheroid with an imperfect interface

This section focuses on a composite spheroid made up with a homogeneous core surrounded by an imperfect interface of LC or HC type. It is obviously a particular case of the more general exact solution derived in section 2 with $N = 1$ ([20], [21], [42]). For finite values of the (LC or HC) interface property, the equivalent conductivity of such a particle in the sense of (76) is actually not independent of the matrix property in an Eshelby problem. However the exact solution requires a rather heavy calculation involving infinite series of harmonics instead of which some approximations can be derived based on simplifying assumptions. The present section aims at reviewing some of

them which are already published and proposing a generalized framework allowing to build new ones. For the sake of simplicity, in the following, the matrix conductivity is denoted by $\boldsymbol{k}_m$ instead of $\boldsymbol{k}_2$, the core conductivity by $\boldsymbol{k}_c$ instead of $\boldsymbol{k}_1$ and the subscript is omitted in the properties of the interface (α or β instead of α_1 or β_1). For further convenience the matrix and core resistivities $\boldsymbol{r}_m = \boldsymbol{k}_m^{-1}$ and $\boldsymbol{r}_c = \boldsymbol{k}_c^{-1}$ are also introduced. The particle domain is denoted by $\mathcal{E}$.

In the literature, the problem of the spheroid (or even ellipsoid) with interface is usually tackled under two different angles : either the interface is seen as in the exact solution as a surface with surface properties ([27], [28], [29], [30], [31]) or it corresponds to the limit of an interphase of (heterogeneous) thickness tending towards 0 with adapted conductivity according to the LC or HC type ([32], [33], [34], [35]).

4.3.1. Interface modelled as a surface

It has been shown that the temperature gradient as well as the heat flux vector remain uniform within a sphere or circular cylinder surrounded by a HC or LC interface and submitted to a remote temperature gradient even in presence of anisotropic materials (see [27] for HC and [28] for LC interface). Nevertheless this result does not hold in the general ellipsoidal case. Indeed in a spheroid, as shown in section 2, these fields are heterogeneous in the core due to the existence of regular terms of degree strictly greater than 1 which are involved when the interface is imperfect. However approximations of the concentration tensor averages have been proposed in [29] for LC interface and in [31] for HC interface based on the use of integral solutions incorporating relevant discontinuities in which heterogeneous temperature gradient (HC case) or heat flux vector (LC case) are replaced by their averages within the particle. These approximations can be easily retrieved thanks to the concept of the (approximated here) equivalent conductivity tensor introduced in (77).

In the case of LC interface, the average of the temperature gradient within the particle (comprising the interface) is decomposed in a regular term and a surface term involving the temperature discontinuity

$$< \underline{h} >_{\mathcal{E}} = -\boldsymbol{r}_c \cdot < \underline{u} >_{\mathcal{E}} + \frac{1}{|\mathcal{E}|} \int_{\partial\mathcal{E}} [\![T]\!] \, \underline{e}_q \, \mathrm{d}S = -\boldsymbol{r}_c \cdot < \underline{u} >_{\mathcal{E}} - \frac{\alpha}{|\mathcal{E}|} \int_{\partial\mathcal{E}} \underline{e}_q \otimes \underline{e}_q \cdot \underline{u} \, \mathrm{d}S \tag{78}$$

For a spherical (or circular particle in 2D), the heat flux vector can rigorously be replaced by its average over $\mathcal{E}$ in the last integral of (78) thanks to the relationship between the position vector and the unit normal vector ($\underline{x} = r\underline{e}_q$ where r is the radius) and to (1a). For an arbitrary ellipsoidal shape, this replacement is not allowed but is invoked in [29] as a simplifying assumption yielding in the case of a spheroid (i.e. using spheroidal notations)

$$< \underline{h} >_{\mathcal{E}} \approx -\boldsymbol{r}_{LC}^{eq} \cdot < \underline{u} >_{\mathcal{E}} \quad \text{with} \quad \boldsymbol{r}_{LC}^{eq} = \boldsymbol{k}_{LC}^{eq\,-1} = \boldsymbol{r}_c + \alpha \boldsymbol{R} \quad \text{and} \quad \boldsymbol{R} = \frac{1}{|\mathcal{E}|} \int_{\partial\mathcal{E}} \underline{e}_q \otimes \underline{e}_q \, \mathrm{d}S \tag{79}$$

Noticeably, unlike the exact solution, this equivalent conductivity does not depend on the conductivity of the matrix and is valid even in the case of anisotropic materials. In addition, inserting $\boldsymbol{k}^{eq}$ given by (79) in (77) exactly boils down to the concentration averages presented in [29] and usable in homogenization schemes. For practical implementation the second-order tensor $\boldsymbol{R}$ can easily be calculated thanks to (A.6) and (A.7) for a spheroid of axis parallel to $\underline{e}_3$

$$\boldsymbol{R} = R_t \left(\mathbf{1} - \underline{e}_3 \otimes \underline{e}_3 \right) + R_a \, \underline{e}_3 \otimes \underline{e}_3 \tag{80}$$

with

$$R_t = \begin{cases} \frac{3}{4} \dfrac{q\left((2-q^2)\,\operatorname{arcsin}\frac{1}{q} + \sqrt{q^2-1}\right)}{c\,\sqrt{q^2-1}} & \text{(prolate)} \\ \frac{3}{4} \dfrac{\tau\left((\tau^2+2)\,\operatorname{arcsinh}\frac{1}{\tau} - \sqrt{\tau^2+1}\right)}{\bar{c}\,\sqrt{\tau^2+1}} & \text{(oblate)} \end{cases} \quad ; \quad R_a = \begin{cases} \frac{3}{2} \dfrac{q^2\,\sqrt{q^2-1}\,\operatorname{arcsin}\frac{1}{q} - (q^2-1)}{c\,q} & \text{(prolate)} \\ \frac{3}{2} \dfrac{\tau^2+1-\tau^2\,\sqrt{\tau^2+1}\,\operatorname{arcsinh}\frac{1}{\tau}}{\bar{c}\,\tau} & \text{(oblate)} \end{cases} \tag{81}$$

where q (resp. τ) is the parameter defining the boundary of the prolate (resp. oblate) spheroid (see AppendixA). The expressions (81) may as well be converted as functions of the aspect ratio and small radius thanks to (A.4) (resp. (A.5))

$$R_t = \begin{cases} \frac{3}{4} \dfrac{\omega\left((\omega^2-2)\,\arctan\sqrt{\omega^2-1} + \sqrt{\omega^2-1}\right)}{b\,(\omega^2-1)^{3/2}} & \text{(prolate)} \\ \frac{3}{4} \dfrac{\omega^2\left((2-\omega^2)\,\operatorname{arctanh}\sqrt{1-\omega^2} - \sqrt{1-\omega^2}\right)}{b\,(1-\omega^2)^{3/2}} & \text{(oblate)} \end{cases} \quad ; \quad R_a = \begin{cases} \frac{3}{2} \dfrac{\omega^2\,\arctan\sqrt{\omega^2-1} - \sqrt{\omega^2-1}}{b\,\omega\,(\omega^2-1)^{3/2}} & \text{(prolate)} \\ \frac{3}{2} \dfrac{\sqrt{1-\omega^2} - \omega^2\,\operatorname{arctanh}\sqrt{1-\omega^2}}{b\,(1-\omega^2)^{3/2}} & \text{(oblate)} \end{cases} \tag{82}$$

Note from (79) that the trace $\mathrm{tr}\,\boldsymbol{R} = 2\,R_t + R_a$ is the specific surface σ_v of the spheroid defined in (A.10). In addition the following limits may be valuable to assess the effect of extreme aspect ratios

$$\left\{\begin{array}{lll} R_t & \underset{\omega\to\infty}{\to} & \frac{3\pi}{8\,b} \\ R_t & \underset{\omega\to 1}{\to} & \frac{1}{b} \\ R_t & \underset{\omega\to 0}{\sim} & -\frac{3}{2\,b}\,\omega^2\,\ln\omega \end{array}\right. \quad ; \quad \left\{\begin{array}{lll} R_a & \underset{\omega\to\infty}{\sim} & \frac{3\pi}{4\,b}\,\omega^{-2} \\ R_a & \underset{\omega\to 1}{\to} & \frac{1}{b} \\ R_a & \underset{\omega\to 0}{\to} & \frac{3}{2\,b} \end{array}\right. \tag{83}$$

The case of HC interface boiling down to the solution unfolded in [31] starts from the average over $\mathcal{E}$ of the heat flux vector. This average comprises a regular term corresponding to the interior of $\mathcal{E}$ as well as a concentrated surface heat flux writing $\underline{u}_s = -\beta(\mathbf{1} - \underline{e}_q \otimes \underline{e}_q)\cdot\underline{h}$ in the tangent plane of $\partial\mathcal{E}$

$$<\underline{u}>_{\mathcal{E}} = -\boldsymbol{k}_c\cdot<\underline{h}>_{\mathcal{E}} + \frac{1}{|\mathcal{E}|}\int_{\partial\mathcal{E}}\underline{u}_s\,\mathrm{d}S = -\boldsymbol{k}_c\cdot<\underline{h}>_{\mathcal{E}} - \frac{\beta}{|\mathcal{E}|}\int_{\partial\mathcal{E}}(\mathbf{1} - \underline{e}_q\otimes\underline{e}_q)\cdot\underline{h}\,\mathrm{d}S \tag{84}$$

Here again it could be shown that a choice of sphere for $\mathcal{E}$ would allow to replace $\underline{h}$ in the last integral of (84) by its average over $\mathcal{E}$. This would not be true for an arbitrary ellipsoid but it is used as a simplifying assumption in [31], which gives for a spheroid

$$<\underline{u}>_{\mathcal{E}} \approx -\boldsymbol{k}^{eq}_{HC}\cdot<\underline{h}>_{\mathcal{E}} \quad \text{with} \quad \boldsymbol{k}^{eq}_{HC} = \boldsymbol{r}^{eq\ -1}_{HC} = \boldsymbol{k}_c + \beta\boldsymbol{L} \quad \text{and} \quad \boldsymbol{L} = \frac{1}{|\mathcal{E}|}\int_{\partial\mathcal{E}}\mathbf{1} - \underline{e}_q\otimes\underline{e}_q\,\mathrm{d}S = (\mathrm{tr}\,\boldsymbol{R})\mathbf{1} - \boldsymbol{R} \tag{85}$$

where the tensor $\boldsymbol{R}$ is defined in (79) and expressed in (80)-(81). Here again this equivalent conductivity does not depend on the matrix property on the contrary to the exact solution and remains valid in the framework of anisotropic materials. Introducing (85) in (77) exactly boils down to the concentration averages presented in [31] and usable in homogenization schemes. The extreme cases of the transverse and axial components of $\boldsymbol{L}$ ($L_t = R_t + R_a$ and $L_a = 2R_t$) are given by

$$\left\{\begin{array}{lll} L_t & \underset{\omega\to\infty}{\to} & \frac{3\pi}{8\,b} \\ L_t & \underset{\omega\to 1}{\to} & \frac{2}{b} \\ L_t & \underset{\omega\to 0}{\to} & \frac{3}{2\,b} \end{array}\right. \quad ; \quad \left\{\begin{array}{lll} L_a & \underset{\omega\to\infty}{\to} & \frac{3\pi}{4\,b} \\ L_a & \underset{\omega\to 1}{\to} & \frac{2}{b} \\ L_a & \underset{\omega\to 0}{\sim} & -\frac{3}{b}\,\omega^2\,\ln\omega \end{array}\right. \tag{86}$$

4.3.2. Interface modelled as a thin interphase

The replacement of an interface by an interphase $\mathcal{I}$ defined as a fictitious volume obtained by extruding the surface of a core $\mathcal{C}$ along its normal is often applied in the literature to a sphere or a circular cylinder with a uniform interphase thickness t [15]. The consistency between the 2D and 3D points of view relies on the fact that the conductivity of the fictitious interphase is built as an isotropic tensor $\boldsymbol{k}_{\mathcal{I}} = k_{\mathcal{I}}\mathbf{1}$ where $k_{\mathcal{I}}$ is a function of the surface property and the uniform thickness t as recalled in [35] (and leading to size effect since a length is introduced)

$$k_{\mathcal{I}} = \frac{t}{\alpha}\ \text{(LC interface)} \quad ; \quad k_{\mathcal{I}} = \frac{\beta}{t}\ \text{(HC interface)} \tag{87}$$

On the one hand, the same strategy can hardly be applied to an arbitrary ellipsoidal shape of the core $\mathcal{C}$. Indeed the extrusion of an ellipsoid normal to its surface with a uniform thickness (or equivalently the Minkowski sum of an ellipsoid and a ball) is in general not an ellipsoid anymore. Conversely the thickness between two concentric coaxial ellipsoids is in general not uniform except between spheres or circular cylinders. On the other hand, while giving up the hypothesis of uniform thickness it seems very tempting to consider that the interphase is a homogeneous material (of isotropic conductivity discussed later) comprised between two concentric and coaxial ellipsoids and take advantage of the general formula (74) defining the PCW bound which is rewritten here

$$\boldsymbol{k}^{eq} = \boldsymbol{k}_{\mathcal{I}} + f_c\left((\boldsymbol{k}_c - \boldsymbol{k}_{\mathcal{I}})^{-1} + \left(\boldsymbol{S}^c - f_c\,\boldsymbol{S}^{\mathcal{I}}\right)\cdot\boldsymbol{k}_{\mathcal{I}}^{-1}\right)^{-1} \quad \text{with} \quad f_c = \frac{|\mathcal{C}|}{|\mathcal{C}| + |\mathcal{I}|} \tag{88}$$

where the volume ratio f_c is therefore close to 1 and $\boldsymbol{S}^c$ (resp. $\boldsymbol{S}^{\mathcal{I}}$) is the Eshelby tensor depending on the shape of the internal (resp. external) ellipsoid in an isotropic matrix. In the case of spheroids, it has been shown in section (3.3) that this expression exactly corresponds to that providing the equivalent conductivity of a confocal two-layer spheroid. Nevertheless (88) can possibly be exploited in a more general situation of ellipsoidal shapes and anisotropic behaviors, when only looking for an *estimate* of the equivalent conductivity.

It is worth noticing that the same formula can be retrieved from an alternative reasoning implemented in [36] in elasticity and [35] in conductivity. This approach is based on a simplifying assumption of uniform temperature gradient $\underline{h}_c$ in the core and a thin thickness between the two ellipsoids. At any point $\underline{x}_\perp$ of the core boundary of unit outward normal $\underline{n}$, the variable thickness denoted by $w(\underline{x}_\perp)$ is defined as the length of the segment of interphase points starting from $\underline{x}_\perp$ and parallel to $\underline{n}$ (see figure 6). Furthermore the temperature gradient at any point $\underline{x}$ of this segment is approximated by its value at the projection $\underline{x}_\perp$ which can itself be deduced from $\boldsymbol{h}_c$ thanks to (E.4)

$$\forall \underline{x} \in \mathcal{I},\ \underline{h}(\underline{x}) \approx \underline{h}(\underline{x}_\perp) = \underline{h}_c + \boldsymbol{\Pi}_{\mathcal{I}}(\underline{n}) \cdot (\boldsymbol{k}_c - \boldsymbol{k}_{\mathcal{I}}) \cdot \underline{h}_c \quad \text{with} \quad \boldsymbol{\Pi}_{\mathcal{I}}(\underline{n}) = \frac{\underline{n} \otimes \underline{n}}{\underline{n} \cdot \boldsymbol{k}_{\mathcal{I}} \cdot \underline{n}} \tag{89}$$

It is then possible to calculate the average of $\underline{h}$ over $\mathcal{I}$ as follows

$$< \underline{h} >_{\mathcal{I}} = \frac{1}{|\mathcal{I}|} \int_{\mathcal{I}} \underline{h}(\underline{x})\, \mathrm{d}\Omega_x \approx \frac{1}{|\mathcal{I}|} \int_{\partial C} \underline{h}(\underline{x}_\perp) w(\underline{x}_\perp)\, \mathrm{d}S_x = \underline{h}_c + \left(\frac{1}{|\mathcal{I}|} \int_{\partial C} \boldsymbol{\Pi}_{\mathcal{I}}(\underline{n}) w(\underline{x}_\perp)\, \mathrm{d}S_x \right) \cdot (\boldsymbol{k}_c - \boldsymbol{k}_{\mathcal{I}}) \cdot \underline{h}_c \tag{90}$$

The integral of the interfacial operator can then be obtained by a judicious application of (F.2b) and Fubini theorem

$$\int_{\partial C} \boldsymbol{\Pi}_{\mathcal{I}}(\underline{n}) w(\underline{x}_\perp)\, \mathrm{d}S_x \approx \int_{\underline{x} \in \mathcal{I}} \left(\boldsymbol{S}^c \cdot \boldsymbol{k}_{\mathcal{I}}^{-1} - \int_{\underline{x}' \in C} \boldsymbol{\Gamma}_{\mathcal{I}}(\underline{x} - \underline{x}')\, \mathrm{d}\Omega'_x \right) \mathrm{d}\Omega_x = |\mathcal{I}|\, \boldsymbol{S}^c \cdot \boldsymbol{k}_{\mathcal{I}}^{-1} - \int_{\underline{x}' \in C} \int_{\underline{x} \in \mathcal{I}} \boldsymbol{\Gamma}_{\mathcal{I}}(\underline{x} - \underline{x}')\, \mathrm{d}\Omega_x\, \mathrm{d}\Omega'_x \tag{91}$$

The integration over $\mathcal{I}$ by $\underline{x}$ in this last expression can be decomposed as a difference between an integration over the whole ellipsoid $\mathcal{I} \cup C$ and an integration over C. In both cases, the other variable $\underline{x}'$ remains interior with respect to the domain covered by $\underline{x}$ so that (F.2a) applies twice to give

$$\int_{\partial C} \boldsymbol{\Pi}_{\mathcal{I}}(\underline{n}) w(\underline{x}_\perp)\, \mathrm{d}S_x \approx \left(|\mathcal{I}|\, \boldsymbol{S}^c - |C|\, (\boldsymbol{S}^{\mathcal{I}} - \boldsymbol{S}^c) \right) \cdot \boldsymbol{k}_{\mathcal{I}}^{-1} = |\mathcal{I}|\, \frac{\boldsymbol{S}^c - f_c\, \boldsymbol{S}^{\mathcal{I}}}{1 - f_c} \cdot \boldsymbol{k}_{\mathcal{I}}^{-1} \tag{92}$$

Introducing (92) in (90) yields

$$< \underline{h} >_{\mathcal{I}} = \left(\boldsymbol{1} + \frac{\boldsymbol{S}^c - f_c\, \boldsymbol{S}^{\mathcal{I}}}{1 - f_c} \cdot \boldsymbol{k}_{\mathcal{I}}^{-1} \cdot (\boldsymbol{k}_c - \boldsymbol{k}_{\mathcal{I}}) \right) \cdot \underline{h}_c \tag{93}$$

and

$$< \underline{h} >_{\mathcal{I} \cup C} = f_c\, \underline{h}_c + (1 - f_c)\ < \underline{h} >_{\mathcal{I}} = \left(\boldsymbol{1} + \left(\boldsymbol{S}^c - f_c\, \boldsymbol{S}^{\mathcal{I}} \right) \cdot \boldsymbol{k}_{\mathcal{I}}^{-1} \cdot (\boldsymbol{k}_c - \boldsymbol{k}_{\mathcal{I}}) \right) \cdot \underline{h}_c \tag{94}$$

Finally the equivalent conductivity can be identified after the calculation of the average heat flux vector over the whole particle $\mathcal{I} \cup C$

$$< \underline{u} >_{\mathcal{I} \cup C} = -f_c\, \boldsymbol{k}_c \cdot \underline{h}_c - (1 - f_c)\, \boldsymbol{k}_{\mathcal{I}} \cdot < \underline{h} >_{\mathcal{I}} = -\boldsymbol{k}_{\mathcal{I}} \cdot < \underline{h} >_{\mathcal{I} \cup C} - f_c\ (\boldsymbol{k}_c - \boldsymbol{k}_{\mathcal{I}}) \cdot \underline{h}_c \tag{95}$$

in which $\underline{h}_c$ can be expressed with respect to $< \underline{h} >_{\mathcal{I} \cup C}$ thanks to (94) so that (95) rewrites in a form putting in evidence an equivalent conductivity identical to (88)

$$< \underline{u} >_{\mathcal{I} \cup C} = -\left(\boldsymbol{k}_{\mathcal{I}} + f_c \left((\boldsymbol{k}_c - \boldsymbol{k}_{\mathcal{I}})^{-1} + \left(\boldsymbol{S}^c - f_c\, \boldsymbol{S}^{\mathcal{I}} \right) \cdot \boldsymbol{k}_{\mathcal{I}}^{-1} \right)^{-1} \right) \cdot < \underline{h} >_{\mathcal{I} \cup C} \tag{96}$$

Once in possession of an equivalent conductivity of the type (88), it is now time to discuss about, on the one hand, the identification of a relevant conductivity for the interphase keeping in mind that the thickness of the interphase is

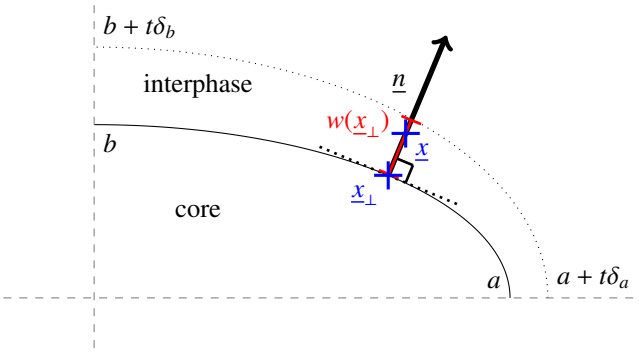

Figure 6: Ellipsoid coated with a thin interphase

not uniform and, on the other hand, the choice of the shape of the ellipsoids defining $\boldsymbol{S}^c$ and $\boldsymbol{S}^I$. The shape of the core is guided by that of the actual modelled particle but that of the external ellipsoid ruling the thickness distribution of the interphase is undetermined and shall be adjusted according to modelling hypotheses. The only constraint is that the thickness remains infinitesimal compared to the core dimensions. The idea here consists in introducing a parameter t, having the dimension of a length, tending towards 0 (i.e. infinitesimal compared to the radii) and governing both the interphase conductivity still in the form (87) (for either LC or HC cases even if t is not the thickness anymore) and the shape of the external ellipsoid. Although the following reasoning could be followed for general ellipsoidal shapes, it is restricted to spheroids for the sake of simplicity and to allow further comparisons with the exact solution provided in section 2. If a and b respectively denote the large and small radii of the core, the radii of the external spheroid (concentric and coaxial to the core) are defined by $a + t\delta_a$ and $b + t\delta_b$ so that $t\delta_a$ and $t\delta_b$ correspond to the thickness of the interphase along the large and small radii. These two independent dimensionless parameters δ_a and δ_b actually control how the external spheroid tends towards the core when t tends towards 0 and consequently the equivalent conductivity (88). Indeed in this expression of $\boldsymbol{k}^{eq}$ the dependence of $\boldsymbol{k}_I$ on t is known in (87) but f_c and $\boldsymbol{S}^I$ are also functions of t through the values of the radii of the external spheroid ($a + t\delta_a$ and $b + t\delta_b$). Before examining in details the influence of δ_a and δ_b on the limit of $\boldsymbol{k}^{eq}$ when t tends towards 0, it is worth simplifying (88) by introducing the following parameters

$$s = -\frac{\partial f_c}{\partial t}(t=0) \quad \text{and} \quad \boldsymbol{\Sigma} = \frac{\partial \boldsymbol{S}^I}{\partial t}(t=0) \tag{97}$$

Using these notations together with the expressions (87) of k_I leads to the following limits of $\boldsymbol{k}^{eq}$ or $\boldsymbol{r}^{eq} = \boldsymbol{k}^{eq\,-1}$ when t tends towards 0 in the LC and HC cases

$$\boldsymbol{r}^{eq}_{LC} = \boldsymbol{k}^{eq\,-1}_{LC} = \boldsymbol{r}_c + \alpha\,(s\,\boldsymbol{S}^c - \boldsymbol{\Sigma}) \quad \text{and} \quad \boldsymbol{k}^{eq}_{HC} = \boldsymbol{r}^{eq\,-1}_{HC} = \boldsymbol{k}_c + \beta\,(s\,\boldsymbol{1} - (s\,\boldsymbol{S}^c - \boldsymbol{\Sigma})) \tag{98}$$

where the tensor $\boldsymbol{\Sigma}$ is practically calculated by observing from (D.2)-(D.3) that $\boldsymbol{S}^I$ actually depends on t through the aspect ratio ($\omega(t) = \frac{a+t\delta_a}{b+t\delta_b}$ in the prolate case and $\omega(t) = \frac{b+t\delta_b}{a+t\delta_a}$ in the oblate case)

$$\boldsymbol{\Sigma} = \frac{\partial \boldsymbol{S}^I}{\partial \omega}\frac{\partial \omega}{\partial t}(t=0) \tag{99}$$

As the derivative of $\boldsymbol{S}^I$ with respect to ω is provided by (D.4)-(D.5), it follows that the estimates (98) are totally determined by the geometrical parameters $s = -\frac{\partial f_c}{\partial t}$ and $\frac{\partial \omega}{\partial t}$ at $t = 0$ which both write as functions of δ_a and δ_b (for the sake of simplicy ω without argument denotes the aspect ratio at $t = 0$ i.e. the aspect ratio of the core spheroid)

$$f_c(t) = \begin{cases} \frac{a\,b^2}{(a+t\delta_a)\,(b+t\delta_b)^2} & \text{(prolate)} \\ \frac{a^2\,b}{(a+t\delta_a)^2\,(b+t\delta_b)} & \text{(oblate)} \end{cases} \quad \Rightarrow \quad s = -\frac{\partial f_c}{\partial t}(t=0) = \begin{cases} \frac{1}{b}\left(\frac{\delta_a}{\omega} + 2\,\delta_b\right) & \text{(prolate)} \\ \frac{1}{b}\,(2\,\delta_a\,\omega + \delta_b) & \text{(oblate)} \end{cases} \tag{100}$$

and

$$\omega(t) = \begin{cases} \frac{a+t\delta_a}{b+t\delta_b} & \text{(prolate)} \\ \frac{b+t\delta_b}{a+t\delta_a} & \text{(oblate)} \end{cases} \quad \Rightarrow \quad \frac{\partial \omega}{\partial t}(t=0) = \begin{cases} \frac{1}{b}\,(\delta_a - \delta_b\,\omega) & \text{(prolate)} \\ \frac{\omega}{b}\,(\delta_b - \delta_a\,\omega) & \text{(oblate)} \end{cases} \tag{101}$$

As a consequence, the equivalent conductivities (98) are fully determined by any choice of the couple (δ_a, δ_b). Alternatively, as two independent values are required to achieve the determination of the model, it may also be interesting for particular physical meanings to use s or $\frac{\partial \omega}{\partial t}$ themselves or any relevant linear combination of δ_a and δ_b as control parameters. Several options of control parameters are detailed herebelow.

- The choice of δ_a and/or δ_b amounts to a control of the thickness along the corresponding axis. For instance $\delta_a = 1$ gives t the status of interphase thickness along the major axis of the spheroid.
- Imposing $\frac{\partial \omega}{\partial t} = 0$ means that the spheroids delimiting the interphase are similar. It implies a linear combination between δ_a and δ_b

$$\frac{\partial \omega}{\partial t} = 0 \text{ (similar spheroids)} \quad \Rightarrow \quad \begin{cases} \delta_a = \delta_b\,\omega & \text{(prolate)} \\ \delta_b = \delta_a\,\omega & \text{(oblate)} \end{cases} \tag{102}$$

- As an alternative option, the spheroids delimiting the interphase can be chosen as confocal, which means that $(a + t\delta_a)^2 - (b + t\delta_b)^2$ does not depend on t for t close to 0, implying $a\delta_a = b\delta_b$

$$a\delta_a = b\delta_b \text{ (confocal spheroids)} \quad \Rightarrow \quad \begin{cases} \delta_b = \delta_a\,\omega & \text{(prolate)} \\ \delta_a = \delta_b\,\omega & \text{(oblate)} \end{cases} \tag{103}$$

- Another relevant option to control the model of equivalent conductivity relies on the parameter s itself. The definition (97) clearly shows that s is physically consistent with a ratio between a surface and a volume. More particularly, if t was actually the thickness of the interphase, s would be defined as the specific surface σ_v given in (A.10). Even if t does not define a uniform thickness here, it is tempting to impose $s = \sigma_v$. Besides the geometrical relevance of this choice, it is worth pointing out the consistency between the interface models (79) and (85) on the one hand and the interphase ones (98) on the other hand provided that $\boldsymbol{R}$ (of trace σ_v) is identified to $s\,\boldsymbol{S}^c - \boldsymbol{\Sigma}$ (of trace s).

Various models are implemented in the next paragraph, each of them being based on a choice of two independent control parameters among those listed hereabove. In addition the result proven in AppendixF eventually allows to exploit any equivalent conductivity provided by these models in Eshelby-based concentration relationships (77) just as if the overall spheroid was homogeneous.

4.3.3. Comparisons of models

This paragraph aims at proposing a comparison between a selection of approximated models of equivalent conductivity based on the descriptions given in 4.3.1 and in 4.3.2 and the exact solution as unfolded in section 2 considering various levels of conductivity of the reference medium. Indeed although the approximated models do not depend on the latter, it is not the case of the exact solution. This dependence on the reference medium of the exact solution may question the conditions of relevance of approximated models. On the one hand, in the LC case, figures 7 and 8 represent respectively the transverse and axial equivalent *resistivities* normalized by the *resistive* effect of the interface α/b plotted against the aspect ratio of the spheroid. On the other hand, in the HC case, figures 9 and 10 represent respectively the transverse and axial equivalent *conductivities* normalized by the *conductive* effect of the interface β/b plotted against the aspect ratio of the spheroid. Before entering into the details of the approximated models, it is worth remarking in figures 7-10 that the exact solutions (denoted series) actually depend on the reference medium in a way that differs from a component to another and from a type of interface to another. But it may be noticed that all the curves related to the exact solution of a given figure follow a rather similar trend and remain within the same order of

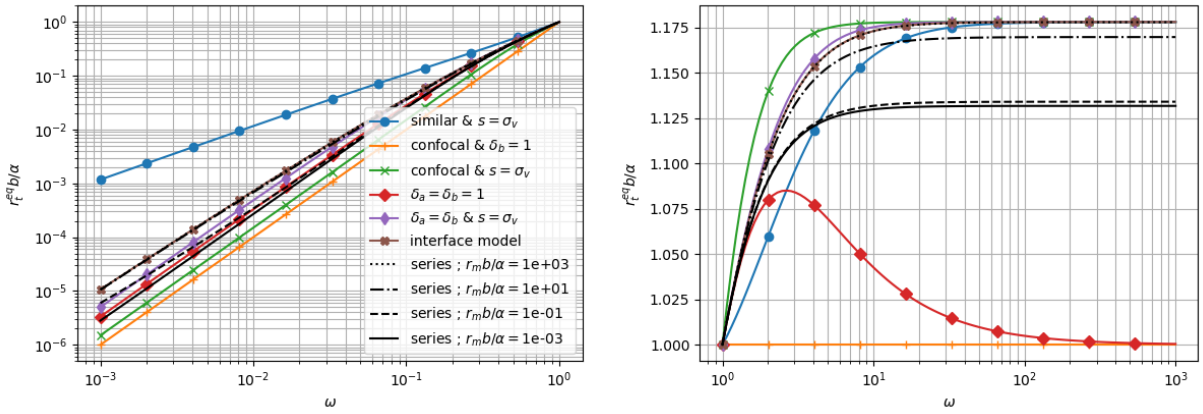

Figure 7: Models of equivalent transverse resistivity of an infinitely conductive spheroid ($r_c = 0$) with LC interface (series truncated at $\mathcal{N} = 5$)

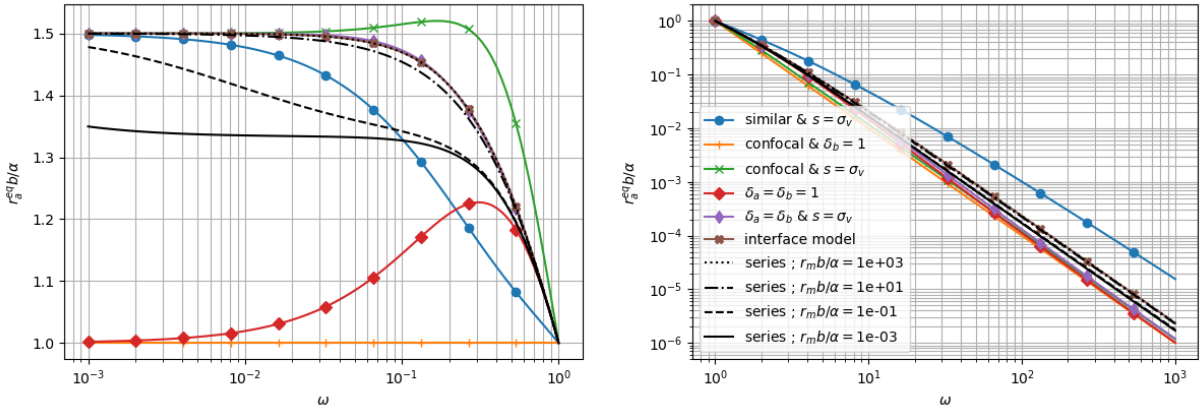

Figure 8: Models of equivalent axial resistivity of an infinitely conductive spheroid ($r_c = 0$) with LC interface (series truncated at $\mathcal{N} = 5$)

magnitude for a given aspect ratio.

Among all possible models, the following ones are considered as a matter of comparison with the exact solution of section 2 and plotted in figures 7 to 10

- *similar spheroids delimiting the interphase* (102) *and specific surface driving the thickness parameter* ($s = \sigma_v$)
  This model is not really satisfactory since its trends in figures 7 (oblate), 8 (prolate) and 10 (oblate) remain far from the exact solution. Moreover the evolutions around the spherical case ($\omega = 1$) almost never comply with the exact solutions either. Other models based on similar spheroids and for instance one of the thicknesses (condition on δ_a or δ_b) are not represented since they behave even worse than this one.

- *confocal spheroids delimiting the interphase* (103) *and small radius control* ($\delta_b = 1$)
  Combining (103) and $\delta_b = 1$ in (100) and (101) provides

$$s = \begin{cases} \frac{1}{b}\left(2 + \frac{1}{\omega^2}\right) \\ \frac{1}{b}\left(1 + 2\,\omega^2\right) \end{cases} \quad \text{and} \quad \frac{\partial \omega}{\partial t} = \begin{cases} \frac{1}{b}\left(\frac{1}{\omega} - \omega\right) & \text{(prolate)} \\ \frac{\omega}{b}\left(1 - \omega^2\right) & \text{(oblate)} \end{cases} \tag{104}$$

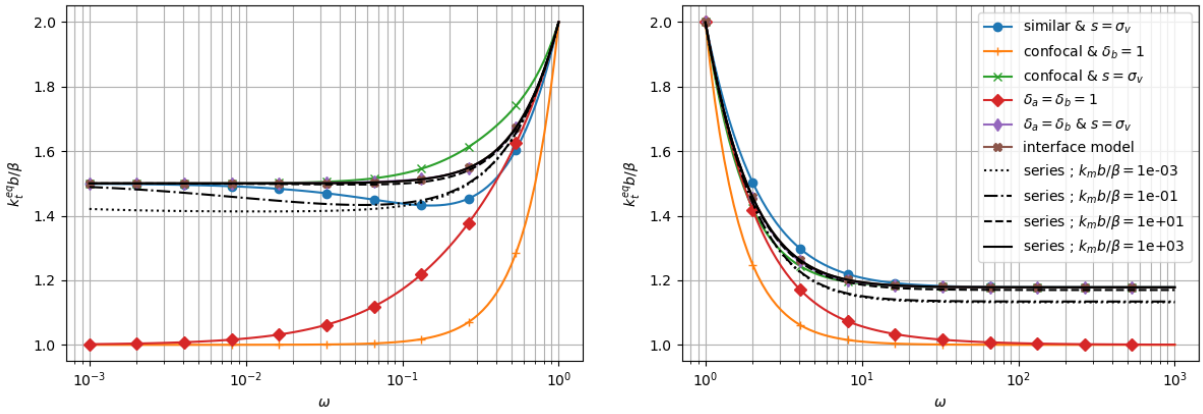

Figure 9: Models of equivalent transverse conductivity of an infinitely resistive spheroid ($k_c = 0$) with HC interface (series truncated at $\mathcal{N} = 5$)

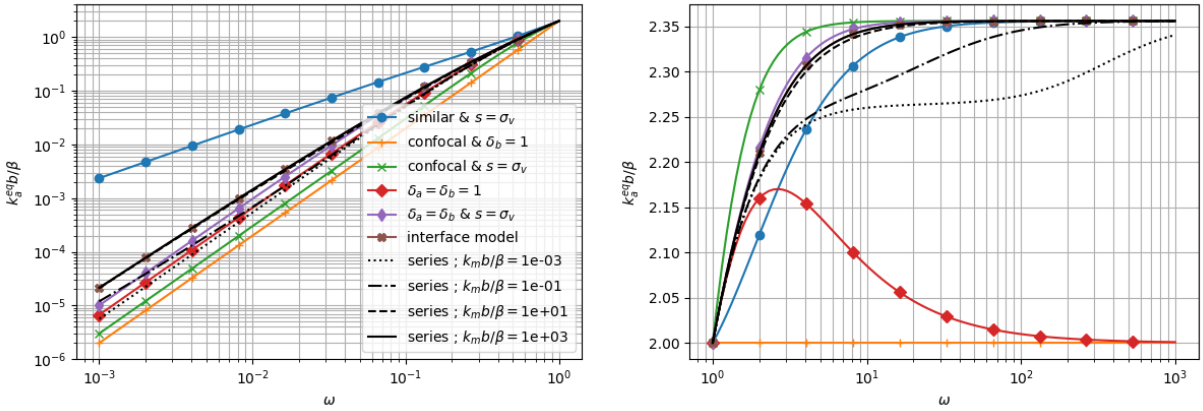

Figure 10: Models of equivalent axial conductivity of an infinitely resistive spheroid ($k_c = 0$) with HC interface (series truncated at $\mathcal{N} = 5$)

The figures put well in evidence that this model is not accurate enough in comparison to the exact solutions whatever the reference medium. Moreover replacing the small radius control $\delta_b = 1$ by a large radius control $\delta_a = 1$ leads to inconsistent results since in this case δ_b (103) and s (100) as well as $\frac{\partial\omega}{\partial t}$ (101) tend to infinite values for extreme cases of needles and flat spheroids.

- *confocal spheroids delimiting the interphase* (103) *and specific surface driving the thickness parameter* ($s = \sigma_v$) Taking advantage of the relationships (103) and (100), $\frac{\partial\omega}{\partial t}$ can be calculated as a function of σ_v so that the following control parameters are valid for oblate or prolate spheroids

$$s = \sigma_v \quad \text{and} \quad \frac{\partial\omega}{\partial t} = \frac{\omega\left(1-\omega^2\right)}{1+2\,\omega^2}\,\sigma_v \tag{105}$$

This set of assumptions is consistent with the model of coated particle presented in [34] for a general ellipsoidal shape and exploited in several homogenization schemes. The figures 7 to 10 show that this model could be acceptable for cases of spheroids rather far from the spherical shape but the trends of the equivalent conductivity do not really comply with the slopes of the exact solutions in the vicinity of $\omega = 1$ in figure 7 prolate, figure 8 oblate, figures 9 oblate and prolate and figure 10 prolate. The latter figures correspond to cases where the

equivalent resistivity (if LC interface) or conductivity (if HC interface) tends towards a non-zero limit whereas the other figures are presented with a logarithmic scale on the y-axis in order to capture the order of convergence towards 0.

- *double radius control ($\delta_a = \delta_b = 1$)*
  Exploiting $\delta_a = \delta_b = 1$ in (100) and (101) gives the parameters to introduce in (98)

$$s = \begin{cases} \frac{1}{b}\left(2 + \frac{1}{\omega}\right) \\ \frac{1}{b}\,(1 + 2\,\omega) \end{cases} \quad \text{and} \quad \frac{\partial \omega}{\partial t} = \begin{cases} \frac{1}{b}\,(1 - \omega) & \text{(prolate)} \\ \frac{\omega}{b}\,(1 - \omega) & \text{(oblate)} \end{cases} \tag{106}$$

  This model means that t is the thickness at both major and minor axes but it is worth recalling that the interphase thickness here remains not uniform so far, even if t is infinitesimal as mistakenly argued in [33]. By the way if the thickness was uniform s given in (106) should coincide with σ_v (A.10), which is not the case when the aspect ratio differs from 1.
  Keeping an aspect ratio in a close vicinity of the spherical case, the figures 7 to 10 show that this model could be acceptable as already put in evidence in [35] using $0.25 \leq \omega \leq 2$. However, when the aspect ratio is far from 1, the discrepancy between this model and the exact solutions increases in cases where the equivalent resistivity (LC interface) or conductivity (HC interface) tends towards a non-zero limit (figure 7 prolate, figure 8 oblate, figures 9 oblate and prolate and figure 10 prolate). Interestingly it is to be noticed that in these cases the interval of validity of the present model is roughly the complementary of the previous one (based on confocal spheroids and a specific surface to control the thickness) which was observed to give more reliable estimates far from the spherical shape.
  As already emphasized in section 4.3.2, the assumption of double radius control contains two independent parameters and thus definitely determines the values of s and $\frac{\partial \omega}{\partial t}$ and eventually the equivalent conductivity (98). Nevertheless the equivalent conductivity formulated in [32] and [33] corresponds to a superposition of $\delta_a = \delta_b = 1$ together with $\boldsymbol{\Sigma} = \mathbf{0}$ (i.e. $\frac{\partial \omega}{\partial t} = 0$). This set of assumptions is geometrically inconsistent since it comes from (101) that $\frac{\partial \omega}{\partial t} \neq 0$ when $\delta_a = \delta_b = 1$ and $\omega \neq 1$; this is certainly the main reason why the model of [32] has been criticized in [42]. The appropriate correction with the right value of $\frac{\partial \omega}{\partial t}$ from (101) actually provides a far more acceptable result.

- *double radius control ($\delta_a = \delta_b$) and specific surface driving the thickness parameter ($s = \sigma_v$)*
  Using $\delta_a = \delta_b$ in (100) with $s = \sigma_v$ and (101) allows to eliminate δ_a and δ_b so that the following parameters to introduce in (98) are obtained for both prolate and oblate spheroids

$$s = \sigma_v \quad \text{and} \quad \frac{\partial \omega}{\partial t} = \frac{\omega\,(1 - \omega)}{1 + 2\,\omega}\,\sigma_v \tag{107}$$

  In this model, the thicknesses at both small and large radii are imposed to be equal to one another but not equal to t. For already mentioned reasons the thickness is however not uniform but its value at radii (i.e. $t\delta_a = t\delta_b$) is somehow corrected by comparison to the previous model imposing $\delta_a = \delta_b = 1$ insofar as it forces the consistency of the thickness with $s = \sigma_v$. The figures 7 to 10 clearly show that this model gives the best estimate of equivalent conductivity among those based on a volume interphase although it can obviously not capture the dependence on the reference medium.

- *interface model*
  The interface model as denominated in the legends of figures 7 to 10 corresponds to the expressions obtained in (79) for LC and in (85) for HC interface. This model remarkably fits well to the exact solution calculated for $r_m b/\alpha$ (LC) or $k_m b/\beta$ (HC) tending towards infinity. This result could have been anticipated since these limits correspond to cases where the effect of the interface becomes negligible relatively to the reference medium, increasing then the validity of the assumption of uniform solution within the spheroid as exploited in section 4.3.1.
  For any finite value of the reference medium, in absence of an efficient strategy to simplify the exact solution while keeping a dependence of the reference medium, it seems that this interface model provides at first sight

the most reliable estimate.
This model also brings indications about the behavior of the equivalent spheroid for extreme aspect ratios thanks to (83) and (86) at least in the case of weak interface effect for which the approximate models are assumed to be close to the exact solutions. Nevertheless these limits should be considered with great care. Indeed the limit of R_t when ω tends towards infinity with a given transverse radius b is $3\pi/(8b)$ and is thus different from the direct application of the integral (79) over a circular cylinder which leads to $1/b$. This means that the transverse solution of an infinite circular cylinder is not obtained here as the limit of the prolate spheroid case which retains even asymptotically its 3D status due to non negligible flow at the tip of the large axis. It is however interesting to notice that the transverse behavior of the infinite circular cylinder is well captured by the two models imposing $\delta_b = 1$ in figures 7 and 9 for ω tending towards infinity, which highlights the expected important role played by the transverse axis (small radius) in this case. A similar reasoning can be applied to the very flat spheroid and the axial conductivity. In this case indeed R_a (83) tends towards $3/(2b)$ whereas the application of the integral (79) on the space delimited by two infinite planes of interdistance $2b$ leads to $1/b$. Here again the conductivity of this last geometry is not obtained by taking the limit of the flat spheroid solution. However the axial conductivity of the space between infinite planes and the major role played by the small radius b are again well captured by the models imposing $\delta_b = 1$ in figures 8 and 10 for ω tending towards 0.

5. Conclusion

The work presented in this paper has been guided by the research of an efficient strategy to enrich the sets of heterogeneities usable in homogenization schemes for thermal conduction with composite spheroidal particles. The analytical solution to the generalized Eshelby problem of a confocal multilayer spheroid with imperfect interfaces between layers has first been provided in the form of different infinite series of spheroidal harmonics for both axial and transverse macroscopic temperature gradients. The coefficients of the series have been identified thanks to a thoroughly detailed procedure allowing a numerical implementation and the convergence of some terms has been carefully justified. The second part of the paper has been dedicated to a specific focus on the case of confocal multilayer spheroid with perfect interfaces. A reformulation of the exact solution expressed this time as finite series of harmonics has been proposed based on the concept of equivalent conductivity satisfying a recursive layer-by-layer algorithm. In particular it has been shown that such a multilayer particle with perfect interfaces between layers could be rigorously replaced by the overall spheroid of uniform transversely isotropic conductivity independently from the properties of the embedding material. However this result of existence of an intrinsic equivalent conduction does not a priori subsist in presence of imperfect interfaces. For this reason and the actual interest for real materials, the issue of the determination of an equivalent property which would be easier to calculate than the series of harmonics has been considered in the third part for the simple case of a uniform spheroid surrounded by an imperfect interface. After some general discussions about the notion of equivalent particle leading to the proof that a composite spheroidal particle could actually be treated as a homogeneous one in terms of expressions of the average concentration tensors, some approximated models have been constructed. These models rely on a replacement of the heterogeneous temperature and heat flux fields within the spheroid by their averages, which is rigorously satisfied when the interface effect vanishes due to Eshelby's result but remains an approximation in presence of an interface. Describing first the interface as a two-dimensional domain has led to already published expressions of concentration tensors. Another approach has consisted in viewing the interface as a thin interphase and applying solutions of multilayer spheroids. Thanks to a parametrization of the shape of this interphase by two scalars, a set of approximated models have been derived. This approach has allowed to discuss about the validity of models published in the literature and to build new ones. Considering oblate and prolate spheroids and LC and HC interfaces, a comparison has finally been carried out between the exact solution and the approximated models in order to highlight the conditions of validity and relevance of the latter. In particular, although independent from the matrix conductivity, it has been put in evidence that the models based on a surface description of the interface probably remain the most accurate ones. It is worth adding that the interest of all the approximated models relies not only on their simplicity but also on their ability to be extended to more general situations such as anisotropy.

Acknowledgements

This work has benefited from fruitful discussions with Prof. Albert Giraud (GeoRessources Laboratory, Université de Lorraine) which are gratefully acknowledged.

AppendixA. Spheroidal coordinates

In the classical cartesian frame of the 3D space $(\underline{e}_1, \underline{e}_2, \underline{e}_3)$, the position vector writes $\underline{x} = x_i \underline{e}_i$ by means of the cartesian coordinates x_i. The prolate spheroidal coordinates of revolution axis $\underline{e}_3$ are defined by the triplet (φ, p, q) [39] such that

$$\left\{ \begin{array}{rcl} x_1 &=& c\,\sqrt{1-p^2}\,\sqrt{q^2-1}\,\cos\varphi \\ x_2 &=& c\,\sqrt{1-p^2}\,\sqrt{q^2-1}\,\sin\varphi \\ x_3 &=& c\,p\,q \end{array} \right. \tag{A.1}$$

with $0 \leq \varphi \leq 2\pi$, $-1 \leq p \leq 1$, $q \geq 1$ and $c > 0$. In other words, the position vector writes

$$\underline{x} = c\left(\sqrt{1-p^2}\,\sqrt{q^2-1}\,\underline{u}_\varphi + p\,q\,\underline{e}_3\right) \quad \text{with} \quad \underline{u}_\varphi = \cos\varphi\,\underline{e}_1 + \sin\varphi\,\underline{e}_2 \tag{A.2}$$

which can also be expressed in terms of spheroidal harmonics by means of Legendre functions of the first kind (B.1b)

$$\underline{x} = c\left(-P_1^1(p)\,P_1^1(q)\,\underline{u}_\varphi + P_1(p)\,P_1(q)\,\underline{e}_3\right) \tag{A.3}$$

The iso-q surfaces define confocal spheroids of linear eccentricity c (semi focal distance), aspect ratio ω, semi major axis a (i.e. axial radius ρ_a) along $\underline{e}_3$ and semi minor axis b (i.e. transverse radius ρ_t) in the plane $(\underline{e}_1, \underline{e}_2)$ given by

$$\omega = \frac{q}{\sqrt{q^2-1}} > 1 \quad \left(q = \frac{\omega}{\sqrt{\omega^2-1}}\right), \quad a = \rho_a = c\,q, \quad b = \rho_t = c\,\sqrt{q^2-1} \tag{A.4}$$

The formal replacement $c = -\imath\bar{c}$ with $\bar{c} > 0$ and $q = \imath\tau$ with $\tau > 0$ and the convention $\sqrt{-1} = \imath$ in (A.1) allows to define the oblate spheroidal coordinates (φ, p, τ) of revolution axis $\underline{e}_3$ corresponding to the linear eccentricity $\bar{c}$. It is worth mentioning that all the results of this paper remain valid by applying this variable replacement and inverting the roles played by a and b in (A.4) in order to keep their respective definitions of semi major and semi minor axes while ρ_a and ρ_t stll respectively denote the axial and transverse radii

$$\omega = \frac{\tau}{\sqrt{\tau^2+1}} < 1 \quad \left(\tau = \frac{\omega}{\sqrt{1-\omega^2}}\right), \quad b = \rho_a = \bar{c}\,\tau \quad a = \rho_t = \bar{c}\,\sqrt{\tau^2+1}, \tag{A.5}$$

The natural basis related to the spheroidal coordinates is defined by the vectors $\underline{a}_\lambda = \partial\underline{x}/\partial\lambda$ where $\lambda = \varphi, p$ or q and the corresponding orthonormal basis $\underline{e}_\lambda$ and Lamé coefficients χ_λ such that $\underline{a}_\lambda = \chi_\lambda \underline{e}_\lambda$ are given by

$$\left\{ \begin{array}{rcl} \chi_\varphi &=& c\,\sqrt{1-p^2}\,\sqrt{q^2-1} \\ \chi_p &=& c\,\sqrt{\frac{q^2-p^2}{1-p^2}} \\ \chi_q &=& c\,\sqrt{\frac{q^2-p^2}{q^2-1}} \end{array} \right. \qquad \left\{ \begin{array}{rcl} \underline{e}_\varphi &=& -\sin\varphi\,\underline{e}_1 + \cos\varphi\,\underline{e}_2 \\ \underline{e}_p &=& \frac{-p\,\sqrt{q^2-1}\,\underline{u}_\varphi + q\,\sqrt{1-p^2}\,\underline{e}_3}{\sqrt{q^2-p^2}} \\ \underline{e}_q &=& \frac{q\,\sqrt{1-p^2}\,\underline{u}_\varphi + p\,\sqrt{q^2-1}\,\underline{e}_3}{\sqrt{q^2-p^2}} \end{array} \right. \tag{A.6}$$

which implies the following expressions of the infinitesimal volume element $\mathrm{d}\Omega$ and surface element $\mathrm{d}S_q$ on an iso-q spheroid

$$\left\{ \begin{array}{rcl} \mathrm{d}\Omega &=& \chi_\varphi\chi_p\chi_q\,\mathrm{d}\varphi\,\mathrm{d}p\,\mathrm{d}q = c^3(q^2-p^2)\,\mathrm{d}\varphi\,\mathrm{d}p\,\mathrm{d}q \\ \mathrm{d}S_q &=& \chi_\varphi\chi_p\,\mathrm{d}\varphi\,\mathrm{d}p = c^2\,\sqrt{q^2-p^2}\,\sqrt{q^2-1}\,\mathrm{d}\varphi\,\mathrm{d}p \end{array} \right. \tag{A.7}$$

The surface of a prolate (resp. oblate) spheroid is given by integration of $\mathrm{d}S_q$ (A.7) over the rectangle $(\varphi, p) \in [0, 2\pi] \times [-1, 1]$ for a given value of q (resp. τ)

$$S = \begin{cases} 2\pi c^2 \sqrt{q^2-1} \left(\sqrt{q^2-1} + q^2 \arcsin \frac{1}{q} \right) & = & 2\pi b^2 \left(1 + \frac{\omega^2}{\sqrt{\omega^2-1}} \arctan \sqrt{\omega^2-1} \right) & \text{(prolate)} \\ 2\pi \bar{c}^2 \sqrt{\tau^2+1} \left(\sqrt{\tau^2+1} + \tau^2 \operatorname{arcsinh} \frac{1}{\tau} \right) & = & 2\pi a^2 \left(1 + \frac{\omega^2}{\sqrt{1-\omega^2}} \operatorname{arctanh} \sqrt{1-\omega^2} \right) & \text{(oblate)} \end{cases} \tag{A.8}$$

and the volume is

$$V = \begin{cases} \frac{4}{3}\pi c^3 q \left(q^2 - 1 \right) & = & \frac{4}{3}\pi b^3 \omega & \text{(prolate)} \\ \frac{4}{3}\pi \bar{c}^3 \tau \left(\tau^2 + 1 \right) & = & \frac{4}{3}\pi a^3 \omega & \text{(oblate)} \end{cases} \tag{A.9}$$

so that the specific surface writes

$$\sigma_v = \frac{S}{V} = \begin{cases} \frac{3}{2cq} \left(1 + \frac{q^2}{\sqrt{q^2-1}} \arcsin \frac{1}{q} \right) & = & \frac{3}{2a} \left(1 + \frac{\omega^2}{\sqrt{\omega^2-1}} \arctan \sqrt{\omega^2-1} \right) & \text{(prolate)} \\ \frac{3}{2\bar{c}\tau} \left(1 + \frac{\tau^2}{\sqrt{\tau^2+1}} \operatorname{arcsinh} \frac{1}{\tau} \right) & = & \frac{3}{2b} \left(1 + \frac{\omega^2}{\sqrt{1-\omega^2}} \operatorname{arctanh} \sqrt{1-\omega^2} \right) & \text{(oblate)} \end{cases} \tag{A.10}$$

In this coordinate system, the surface Laplacian over an iso-q spheroid writes

$$\begin{aligned} \Delta_{\mathcal{S}} f &= \frac{1}{\chi_\varphi \chi_p} \left(\frac{\partial}{\partial \varphi} \left(\frac{\chi_p}{\chi_\varphi} \frac{\partial f}{\partial \varphi} \right) + \frac{\partial}{\partial p} \left(\frac{\chi_\varphi}{\chi_p} \frac{\partial f}{\partial p} \right) \right) \\ &= \frac{1}{c^2} \left(\frac{1}{(1-p^2)(q^2-1)} \frac{\partial^2 f}{\partial \varphi^2} + \frac{1}{\sqrt{q^2-p^2}} \frac{\partial}{\partial p} \left(\frac{1-p^2}{\sqrt{q^2-p^2}} \frac{\partial f}{\partial p} \right) \right) \end{aligned} \tag{A.11}$$

AppendixB. Calculation of integrals

In this appendix, P_n (also written P_n^0) denotes the Legendre polynomial of degree n and P_n^m the associated Legendre function of the first kind of degree n and order m. The following relationships are first recalled for practical convenience [40]

$$\begin{cases} P_0(x) = 1 \; ; \; P_1(x) = x & \text{(B.1a)} \\ P_n^m(x) = \begin{cases} \left(-\sqrt{1-x^2} \right)^m \frac{\mathrm{d}^m P_n(x)}{\mathrm{d}x^m} & (|x| \le 1) \\ \left(\sqrt{x^2-1} \right)^m \frac{\mathrm{d}^m P_n(x)}{\mathrm{d}x^m} & (x > 1) \end{cases} & \text{(B.1b)} \\ P_{n+1}^m(x) = \dfrac{(2n+1)\, x\, P_n^m(x) - (n+m)\, P_{n-1}^m(x)}{n-m+1} \quad (n \ge 1) & \text{(B.1c)} \\ P_{n+1}^{m'}(x) = \dfrac{(2n+1) \left[P_n^m(x) + x P_n^{m'}(x) \right] - (n+m) P_{n-1}^{m'}(x)}{n-m+1} \quad (n \ge 1) & \text{(B.1d)} \\ (1-x^2) P_n''(x) = 2x P_n'(x) + n(n+1) P_n(x) & \text{(B.1e)} \\ \displaystyle\int_{-1}^{1} P_n^m(x) P_r^s(x) \, \mathrm{d}x = \frac{2}{2n+1} \frac{(n+m)!}{(n-m)!} \delta_{nr} \delta_{ms} \quad (n \ge m) & \text{(B.1f)} \end{cases}$$

It may also be useful to recall some of the main formulas allowing to calculate the Legendre functions of the second kind of degree n denoted by Q_n or Q_n^0 as well as the associated Legendre functions of the second kind of

degree n and order m denoted by Q_n^m [40]

$$\begin{cases} Q_0(x) = \begin{cases} \operatorname{arctanh}(x) & (|x| \leq 1) \\ \operatorname{arccoth}(x) & (x > 1) \end{cases} & \text{(B.2a)} \\ Q_1(x) = x\, Q_0(x) - 1 & \text{(B.2b)} \\ Q_n(x) = P_n(x)\, Q_0(x) - \displaystyle\sum_{k=1}^{n} \frac{P_{k-1}(x)\, P_{n-k}(x)}{k} \quad (n \geq 2) & \text{(B.2c)} \\ Q_n^m(x) = \begin{cases} \left(-\sqrt{1-x^2}\right)^m \frac{\mathrm{d}^m Q_n(x)}{\mathrm{d}x^m} & (|x| \leq 1) \\ \left(\sqrt{x^2-1}\right)^m \frac{\mathrm{d}^m Q_n(x)}{\mathrm{d}x^m} & (x > 1) \end{cases} & \text{(B.2d)} \\ Q_{n+1}^m(x) = \dfrac{(2n+1)\, x\, Q_n^m(x) - (n+m)\, Q_{n-1}^m(x)}{n-m+1} \quad (n \geq 2) & \text{(B.2e)} \\ Q_{n+1}^{m'}(x) = \dfrac{(2n+1)\left[Q_n^m(x) + x\, Q_n^{m'}(x)\right] - (n+m)\, Q_{n-1}^{m'}(x)}{n-m+1} \quad (n \geq 2) & \text{(B.2f)} \end{cases}$$

Calculation of $W_k(q)$

$$W_k(q) = \int_{-1}^{1} \frac{x^{2k}}{\sqrt{q^2-x^2}}\,\mathrm{d}x = q^{2k} \int_{-\arcsin\frac{1}{q}}^{\arcsin\frac{1}{q}} \sin^{2k}\theta\,\mathrm{d}\theta \quad (q > 1) \tag{B.3}$$

Considering the power series $\frac{1}{\sqrt{1-z^2}} = \sum_{n=0}^{\infty} \frac{(1/2)_n}{n!} z^{2n}$ (of radius of convergence 1) where $(\lambda)_n = \frac{\Gamma(\lambda+n)}{\Gamma(\lambda)}$ is the rising Pochhammer symbol and Γ the Gamma function, (B.3) can be rewritten as

$$W_k(q) = \frac{2}{q} \sum_{n=0}^{\infty} \frac{(1/2)_n}{n!\,(2n+2k+1)} \frac{1}{q^{2n}} = \frac{2}{q\,(1+2k)}\, {}_2F_1\left(\frac{1}{2}, \frac{1}{2}+k; \frac{3}{2}+k; \frac{1}{q^2}\right) \tag{B.4}$$

where ${}_2F_1$ is the Gaussian hypergeometric function ${}_2F_1\,(a,b;c;z) = \sum_{n=0}^{\infty} \frac{(a)_n\,(b)_n}{(c)_n\,n!} z^{2n}$ which is implemented in many numerical libraries including arbitrary precision such as the `mpmath` `Python` library [48]. Moreover, (B.4) also allows to deduce the behavior of $W_k(q)$ for high values of k for $q > 1$

$$W_k(q) \underset{k\to\infty}{\sim} \frac{1}{k\,\sqrt{q^2-1}} \tag{B.5}$$

The following useful integrals can as well be identified

$$Y_k(q) = \int_{-1}^{1} x^{2k}\,\sqrt{q^2-x^2}\,\mathrm{d}x = q^2\, W_k(q) - W_{k+1}(q) \tag{B.6}$$

Calculation of $I_{ij}(q)$

As Legendre polynomials of even (respectively odd) degree are sums of even (respectively odd) monomials, it comes that

$$I_{ij}(q) = \int_{-1}^{1} \frac{P_i(x)\, P_j(x)}{\sqrt{q^2-x^2}}\,\mathrm{d}x = \begin{cases} 0 & \text{if } (i+j) \text{ is odd} \\ \sum_{k=0}^{(i+j)/2} \gamma_{2k}^{i,j}\, W_k(q) & \text{if } (i+j) \text{ is even} \end{cases} \tag{B.7}$$

where $\gamma_l^{i,j}$ is the coefficient of x^l in the polynomial $P_i(x)P_j(x)$. Adopting the notation $\gamma^{i,j}$ for the vector of components $\gamma_l^{i,j}$ and the convention $\gamma_l^{i,j} = 0$ for $l < 0$ or $l > i+j$, these coefficients can be practically built thanks to a recursive algorithm deduced from (B.1c)

$$\begin{cases} \gamma_l^{i+1,j} = \frac{2i+1}{i+1}\,\gamma_{l-1}^{i,j} - \frac{i}{i+1}\,\gamma_l^{i-1,j} \quad (0 \leq l \leq i+j+1) \\ \gamma_l^{j,i} = \gamma_l^{i,j} \\ \gamma^{0,0} = [0] \quad ; \quad \gamma^{1,0} = [0,1] \quad ; \quad \gamma^{1,1} = [0,0,1] \end{cases} \tag{B.8}$$

Note the practical calculation of integrals as I_{ij} has already been tackled in the literature (e.g. [20]) resorting to another algorithm than the recursive one (B.8) and without focusing on the numerical accuracy of the summation (B.7) especially if high orders are considered. This is precisely the purpose of AppendixC in which it is shown that this issue actually needs to be investigated.

Calculation of $J_{ij}(q)$

Resorting to an integration by parts and (B.1b) allows to write

$$\begin{aligned} J_{ij}(q) &= \int_{-1}^{1} -P_i(x)\,\frac{\partial}{\partial x}\left(\frac{P'_j(x)\,(1-x^2)}{\sqrt{q^2-x^2}}\right)\mathrm{d}x = \int_{-1}^{1}\frac{P'_i(x)\,P'_j(x)\,(1-x^2)}{\sqrt{q^2-x^2}}\,\mathrm{d}x \\ &= \int_{-1}^{1}\frac{P^1_i(x)\,P^1_j(x)}{\sqrt{q^2-x^2}}\,\mathrm{d}x \\ &= \begin{cases} 0 & \text{if } (i+j) \text{ is odd} \\ \sum_{k=0}^{(i+j)/2-1}\delta^{i,j}_{2\,k}\left(W_k(q)-W_{k+1}(q)\right) & \text{if } (i+j) \text{ is even} \end{cases} \end{aligned} \tag{B.9}$$

where $\delta^{i,j}_l$ is the coefficient of x^l in the polynomial $P'_i(x)P'_j(x)$. In order to build a method to calculate $\delta^{i,j}_l$, it is convenient first to introduce $\eta^{i,j}_l$ as the coefficient of x^l in the polynomial $P'_i(x)P_j(x)$. Unlike $\gamma^{i,j}_l$ and $\delta^{i,j}_l$, $\eta^{i,j}_l$ is not symmetric with respect to i and j but the following recursive algorithm can be established thanks to (B.1c) and (B.1d)

$$\begin{cases} \eta^{i+1,j}_l = \frac{2\,i+1}{i+1}\,\gamma^{i,j}_l + \frac{2\,i+1}{i+1}\,\eta^{i,j}_{l-1} - \frac{i}{i+1}\,\eta^{i-1,j}_l \quad (0 \le l \le i+j) \\ \eta^{i,j+1}_l = \frac{2\,j+1}{j+1}\,\eta^{i,j}_{l-1} - \frac{j}{j+1}\,\eta^{i,j-1}_l \quad (0 \le l \le i+j) \\ \eta^{0,0} = [0] \quad ; \quad \eta^{0,1} = [0] \quad ; \quad \eta^{1,0} = [1] \quad ; \quad \eta^{1,1} = [0,1] \end{cases} \tag{B.10}$$

Finally the algorithm providing $\delta^{i,j}_l$ writes

$$\begin{cases} \delta^{i+1,j}_l = \frac{2\,i+1}{i+1}\,\eta^{j,i}_l + \frac{2\,i+1}{i+1}\,\delta^{i,j}_{l-1} - \frac{i}{i+1}\,\delta^{i-1,j}_l \quad (0 \le l \le i+j-1) \\ \delta^{j,i}_l = \delta^{i,j}_l \\ \delta^{0,0} = [0] \quad ; \quad \delta^{1,0} = [0] \quad ; \quad \delta^{1,1} = [1] \end{cases} \tag{B.11}$$

Calculation of $K_{ij}(q)$

$$K_{ij}(q) = \int_{-1}^{1}\frac{P^{1'}_i(x)\,P^{1'}_j(x)\,(1-x^2)}{\sqrt{q^2-x^2}}\,\mathrm{d}x \tag{B.12}$$

The use of (B.1b) and (B.1e) allows to rewrite (B.12) under the form

$$K_{ij}(q) = \int_{-1}^{1}\frac{P'_i(x)P'_j(x)x^2 - \Big(j(j+1)P'_i(x)P_j(x) + i(i+1)P_i(x)P'_j(x)\Big)x + i(i+1)j(j+1)P_i(x)P_j(x)}{\sqrt{q^2-x^2}}\,\mathrm{d}x \tag{B.13}$$

which is zero if $(i+j)$ is odd and can be transformed into the following summation if $(i+j)$ is even

$$K_{ij}(q) = i(i+1)j(j+1)\gamma^{i,j}_0 W_0(q) + \sum_{k=1}^{(i+j)/2}\Big(\delta^{i,j}_{2k-2} - j(j+1)\eta^{i,j}_{2k-1} - i(i+1)\eta^{j,i}_{2k-1} + i(i+1)j(j+1)\gamma^{i,j}_{2k}\Big)W_k(q) \tag{B.14}$$

Calculation of $L_{ij}(q)$

Using (B.1b), this integral writes

$$L_{ij}(q) = \int_{-1}^{1} \frac{P_i^1(x)\,P_j^1(x)\,\sqrt{q^2-x^2}}{1-x^2}\,\mathrm{d}x = \int_{-1}^{1} P_i'(x)\,P_j'(x)\,\sqrt{q^2-x^2}\,\mathrm{d}x$$
$$= \begin{cases} 0 & \text{if } (i+j) \text{ is odd} \\ \sum_{k=0}^{(i+j)/2-1} \delta_{2k}^{i,j}\Big(q^2\,W_k(q) - W_{k+1}(q)\Big) & \text{if } (i+j) \text{ is even} \end{cases} \tag{B.15}$$

AppendixC. On the numerical convergence of the summations (B.7), (B.9), (B.14) and, (B.15)

Exploiting (B.1f), observing that $\sqrt{q^2-1} \le \sqrt{q^2-x^2} \le q$ and using Cauchy-Schwartz inegality imply

$$\frac{2}{2\,i+1}\,\frac{1}{q} \le I_{ii}(q) \le \frac{2}{2\,i+1}\,\frac{1}{\sqrt{q^2-1}} \quad \text{and} \quad |I_{ij}(q)| \le \sqrt{I_{ii}(q)}\,\sqrt{I_{jj}(q)} \tag{C.1}$$

which allows to bound the order of magnitude of the definite positive symmetric matrix of general term $I_{ij}(q)$ (B.7).

Despite its simplicity of implementation, the algorithm based on the summation (B.7) together with (B.8) and (B.4) hides the fact that some terms of the series in (B.7) are many orders of magnitude higher than $I_{ij}(q)$ when i and j take large values, which may lead to numerical problems. It is then necessary to estimate the order of magnitude of the coefficients $\gamma_l^{i,j}$ and eventually to resort to a specific numerical library such as `mpmath` to control the desired precision if the latter exceeds the standard one (16 digits for double precision) in order to ensure the validity of the numerical calculation of the summation. The reasoning starts by the Rodrigues formula and the binomial expansion

$$P_n(x) = \frac{1}{2^n\,n!}\,\frac{\mathrm{d}^n}{\mathrm{d}x^n}\Big[\big(x^2-1\big)^n\Big] = \sum_{k\ge n/2}^{n} \underbrace{\frac{(-1)^{n-k}\,(2\,k)!}{2^n\,(n-k)!\,k!\,(2\,k-n)!}}_{\theta_k^n}\,x^{2\,k-n} \tag{C.2}$$

The order of magnitude of θ_k^n is then estimated for high values of k and n thanks to the Stirling formula [1]

$$\log|\theta_k^n| \underset{n\to\infty}{\sim} k\log k - (n-k)\,\log(n-k) - (2\,k-n)\,\log(k-n/2) \tag{C.3}$$

An optimization of (C.3) with respect to k finally provides the maximal order of magnitude of θ_k^n

$$\max_k \log|\theta_k^n| \underset{n\to\infty}{\sim} n\,\frac{\log\frac{2+\sqrt{2}}{2-\sqrt{2}}}{2\,(\log 2+\log 5)} \text{ reached for } (2\,k-n) \underset{n\to\infty}{\sim} \frac{n}{\sqrt{2}} \tag{C.4}$$

It follows then that the maximal order of magnitude of the terms in the summation (B.7) is approximated by

$$\max_{\substack{k\\0\le i\le n\\0\le j\le n}} \log|\gamma_{2\,k}^{i,j}| \underset{n\to\infty}{\sim} n\,\frac{\log\frac{2+\sqrt{2}}{2-\sqrt{2}}}{\log 2+\log 5} \le 0.8\,n \tag{C.5}$$

Besides on the one hand it is shown from (B.5) that $\log W_k(q) \underset{k\to\infty}{\sim} -\log k$ which is also equivalent to $-\log n$ if (C.4) is considered. On the other hand it comes from (C.1) that $\log I_{nn}(q) \underset{n\to\infty}{\sim} -\log n$. As a consequence, the construction of the terms $I_{ij}(q)$ for $0 \le i,j \le n$ by means of the summation (B.7) requires to adopt a precision defined by a number of digits at least equal to $\lceil 0.8n\rceil$ where $\lceil . \rceil$ denotes the ceiling function. This estimation is well confirmed by

[1] $n! \underset{n\to\infty}{\sim} \sqrt{2\pi n}(n/e)^n$

numerical calculations presented in Figure C.11 which shows the divergence of $I_{ii}(q)$ as soon as the precision criterion is violated. It is then recommended not to use the summation formula (B.7) for i or j higher than 20 in the framework of double precision or to resort to a multiple precision library with a number of significant digits at least equal to $\lceil 0.8n \rceil$ if n denotes the maximal degree of Legendre polynomials.

The number of significant digits which are necessary to evaluate the other summations (B.9), (B.14) and (B.15) is obviously the same since the order of magnitude (C.4) is also valid for the coefficients of the derivative of Legendre polynomials and consequently the precision (C.5) also applies to the coefficients $\eta_l^{i,j}$ and $\delta_l^{i,j}$.

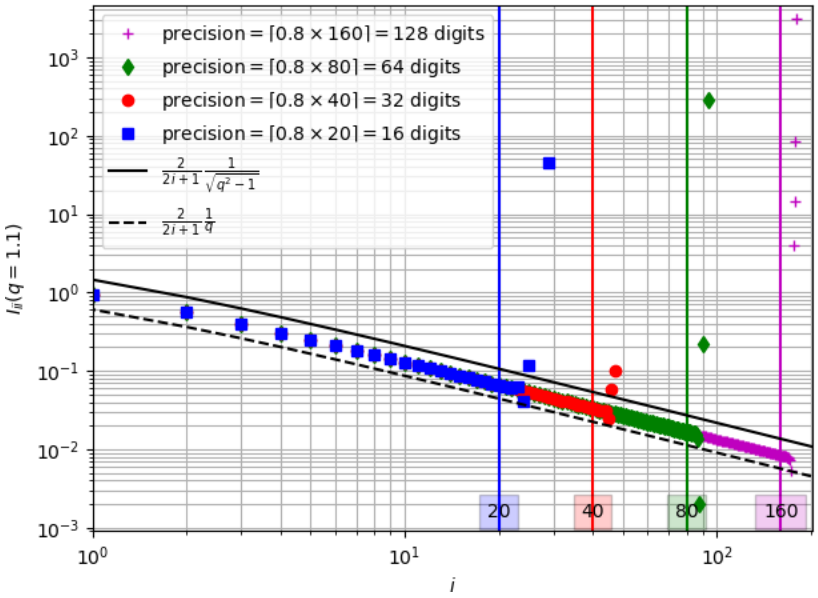

Figure C.11: Influence of the precision level on the calculation of $I_{ii}(q)$ with $q = 1.1$ ($\omega = 2.4$)

AppendixD. Eshelby problem in conduction

This section recalls the expression of the temperature gradient in a spheroidal inhomogeneity of conduction $\boldsymbol{k}_{\mathcal{E}}$ embedded in an infinite matrix of conductivity $\boldsymbol{k}_m$ submitted to a remote temperature gradient $\underline{H}$. From the Eshelby result [2] applied to conductivity, the temperature gradient within the ellipsoidal inhomogeneity $\mathcal{E}$ is homogeneous and writes [1]

$$\forall \underline{x} \in \mathcal{E},\ \underline{h}(\underline{x}) = \left(\mathbf{1} + \boldsymbol{S}_m^{\mathcal{E}} \cdot \boldsymbol{k}_m^{-1} \cdot (\boldsymbol{k}_{\mathcal{E}} - \boldsymbol{k}_m)\right)^{-1} \cdot \underline{H} \tag{D.1}$$

where $\boldsymbol{S}_m^{\mathcal{E}}$ is the Eshelby tensor depending only on the shape of the ellipsoid and the anisotropy of $\boldsymbol{k}_m$. If $\boldsymbol{k}_m$ is isotropic, $\boldsymbol{S}_m^{\mathcal{E}}$ does not depend on the latter and can be simply denoted by $\boldsymbol{S}^{\mathcal{E}}$. In the case of a spheroidal shape of axis parallel to $\underline{e}_3$ and aspect ratio ω, $\boldsymbol{S}^{\mathcal{E}}$ writes [45]

$$\boldsymbol{S}^{\mathcal{E}}(\omega) = S_t^{\mathcal{E}}(\omega)\left(\mathbf{1} - \underline{e}_3 \otimes \underline{e}_3\right) + S_a^{\mathcal{E}}(\omega)\,\underline{e}_3 \otimes \underline{e}_3 \tag{D.2}$$

with (note that $S_a^{\mathcal{E}} = 1 - 2S_t^{\mathcal{E}}$)

$$S_t^{\mathcal{E}}(\omega) = \begin{cases} \frac{\omega\left(\omega\sqrt{\omega^2-1} - \operatorname{arccosh}\omega\right)}{2(\omega^2-1)^{3/2}} & (\omega > 1) \\ \frac{\omega\left(\arccos\omega - \omega\sqrt{1-\omega^2}\right)}{2(1-\omega^2)^{3/2}} & (\omega < 1) \\ \frac{1}{3} & (\omega = 1) \end{cases} ;\ S_a^{\mathcal{E}}(\omega) = \begin{cases} \frac{\omega\operatorname{arccosh}\omega - \sqrt{\omega^2-1}}{(\omega^2-1)^{3/2}} & (\omega > 1) \\ \frac{\sqrt{1-\omega^2} - \omega\arccos\omega}{(1-\omega^2)^{3/2}} & (\omega < 1) \\ \frac{1}{3} & (\omega = 1) \end{cases} \tag{D.3}$$

In addition the derivative of the Eshelby tensor (D.2) with respect to the aspect ratio writes (note that $\frac{\partial S_a^{\mathcal{E}}}{\partial \omega} = -2\frac{\partial S_t^{\mathcal{E}}}{\partial \omega}$)

$$\frac{\partial \boldsymbol{S}^{\mathcal{E}}}{\partial \omega}(\omega) = \frac{\partial S_t^{\mathcal{E}}}{\partial \omega}(\omega)\left(\mathbf{1} - \underline{e}_3 \otimes \underline{e}_3\right) + \frac{\partial S_a^{\mathcal{E}}}{\partial \omega}(\omega)\,\underline{e}_3 \otimes \underline{e}_3 = \frac{\partial S_t^{\mathcal{E}}}{\partial \omega}(\omega)\left(\mathbf{1} - 3\,\underline{e}_3 \otimes \underline{e}_3\right) \tag{D.4}$$

with

$$\frac{\partial S_t^{\mathcal{E}}}{\partial \omega}(\omega) = \begin{cases} \frac{(1+2\,\omega^2)\,\operatorname{arccosh}\omega - 3\,\omega\,\sqrt{\omega^2-1}}{2\,(\omega^2-1)^{5/2}} & (\omega > 1) \\ \frac{(1+2\,\omega^2)\,\arccos\omega - 3\,\omega\,\sqrt{1-\omega^2}}{2\,(1-\omega^2)^{5/2}} & (\omega < 1) \\ \frac{2}{15} & (\omega = 1) \end{cases} ; \frac{\partial S_a^{\mathcal{E}}}{\partial \omega}(\omega) = \begin{cases} \frac{3\,\omega\,\sqrt{\omega^2-1} - (1+2\,\omega^2)\,\operatorname{arccosh}\omega}{(\omega^2-1)^{5/2}} & (\omega > 1) \\ \frac{3\,\omega\,\sqrt{1-\omega^2} - (1+2\,\omega^2)\,\arccos\omega}{(1-\omega^2)^{5/2}} & (\omega < 1) \\ \frac{-4}{15} & (\omega = 1) \end{cases} \tag{D.5}$$

AppendixE. Hadamard jump condition and interfacial operator

The problem considered here is the jump condition of temperature gradient and heat flux vector at an interface point between two zones in the framework of steady state thermal conduction (see figure E.12). On both sides of this interface point the conductivity tensor is $\boldsymbol{k}_m$ and a polarization tensor $\underline{p}$ is defined only in the first zone. Any discontinuity of a quantity $\mathcal{X}$ equal to $\mathcal{X}_1$ in the first zone and $\mathcal{X}_2$ in the second is denoted by $[\![\mathcal{X}]\!] = \mathcal{X}_2 - \mathcal{X}_1$ and the unit normal vector $\underline{n}$ is defined as directed towards the second zone (see figure E.12).

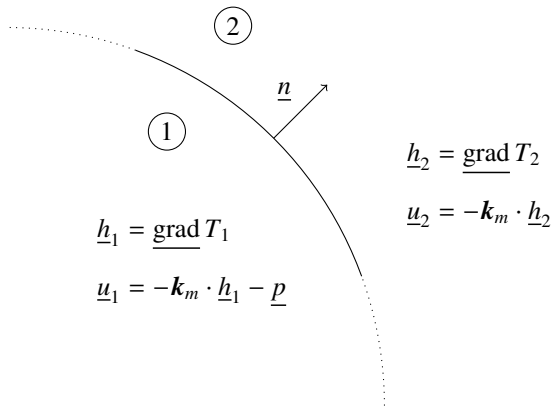

Figure E.12: Hadamard jump condition

The so-called Hadamard jump condition ([49], [50]) results from the continuity of the temperature field over the interface which entails the continuity of the tangential components of the temperature gradient so that there exists a scalar μ such that

$$[\![\,\underline{h}\,]\!] = [\![\,\underline{\operatorname{grad}}\,T\,]\!] = \mu\,\underline{n} \tag{E.1}$$

The determination of μ is finally achieved by exploiting the continuity of the normal heat flux through the interface ($[\![\,\underline{u}\,]\!] \cdot \underline{n} = 0$)

$$\mu\,\underline{n} \cdot \boldsymbol{k}_m \cdot \underline{n} = \underline{n} \cdot \boldsymbol{k}_m \cdot [\![\,\underline{h}\,]\!] = \underline{n}\left(\underline{p} - [\![\,\underline{u}\,]\!]\right) = \underline{n} \cdot \underline{p} \tag{E.2}$$

Replacing μ (E.2) in (E.1) defines the interfacial operator $\boldsymbol{\Pi}_m(\underline{n})$ ([51], [36], [29])

$$\underline{h}_2 = \underline{h}_1 + \boldsymbol{\Pi}_m(\underline{n}) \cdot \underline{p} \quad \text{with} \quad \boldsymbol{\Pi}_m(\underline{n}) = \frac{\underline{n} \otimes \underline{n}}{\underline{n} \cdot \boldsymbol{k}_m \cdot \underline{n}} \tag{E.3}$$

In the case of material discontinuity (i.e. conductivity $\boldsymbol{k}_1$ in zone 1 and $\boldsymbol{k}_2$ in zone 2) without any polarization, $\underline{u}_1$ also rewrites $\underline{u}_1 = -\boldsymbol{k}_2 \cdot \underline{h}_1 - \underline{p}$ with $\underline{p} = (\boldsymbol{k}_1 - \boldsymbol{k}_2) \cdot \underline{h}_1$ so that (E.3) applies with $\boldsymbol{k}_m = \boldsymbol{k}_2$ and the fictitious polarization $\underline{p}$

$$\underline{h}_2 = \underline{h}_1 + \boldsymbol{\Pi}_2(\underline{n}) \cdot (\boldsymbol{k}_1 - \boldsymbol{k}_2) \cdot \underline{h}_1 \quad \text{with} \quad \boldsymbol{\Pi}_2(\underline{n}) = \frac{\underline{n} \otimes \underline{n}}{\underline{n} \cdot \boldsymbol{k}_2 \cdot \underline{n}} \tag{E.4}$$

AppendixF. Integral solution to the generalized Eshelby inclusion problem

This section recalls the solution to the Eshelby inclusion problem corresponding to an infinite domain occupied by a homogeneous material of conductivity $\boldsymbol{k}_m$ embedding an ellipsoidal domain $\mathcal{E}$ of arbitrary (not necessarily uniform) conduction law and subjected to a remote temperature gradient $\underline{H}$. Introducing a fictitious polarization vector field $\underline{p} = -(\boldsymbol{k}_m \cdot \underline{h} + \underline{u})$ within $\mathcal{E}$, the solution writes in the sense of distributions (i.e. the polarization may incorporate surface Dirac distributions due to temperature discontinuities or concentrated heat flux)

$$\underline{h}(\underline{x}) = \underline{H} - \int_{\underline{x}' \in \mathcal{E}} \boldsymbol{\Gamma}_m(\underline{x} - \underline{x}') \cdot \underline{p}(\underline{x}') \, \mathrm{d}\Omega' = \underline{H} + \int_{\underline{x}' \in \mathcal{E}} \boldsymbol{\Gamma}_m(\underline{x} - \underline{x}') \cdot \left(\boldsymbol{k}_m \cdot \underline{h}(\underline{x}') + \underline{u}(\underline{x}') \right) \mathrm{d}\Omega' \tag{F.1}$$

where $\boldsymbol{\Gamma}_m$ is the second-order Green tensor of the conduction problem related to $\boldsymbol{k}_m$ in an infinite medium. If G_m denotes the Green function of the problem defined by $\mathrm{div}(\boldsymbol{k}_m \cdot \underline{\mathrm{grad}}\, G_m) + \delta_0 = 0$ and $\lim_{||\underline{x}|| \to \infty} G_m(\underline{x}) = 0$, then it comes that $\boldsymbol{\Gamma}_m = \boldsymbol{S}_m^{\mathcal{E}} \cdot \boldsymbol{k}_m^{-1} \delta_0 - \mathrm{PV}_{\mathcal{E}}\, \mathbf{hess} G_m$. The first term is a singular part involving a 3D Dirac distribution δ_0 and the Eshelby tensor $\boldsymbol{S}_m^{\mathcal{E}}$ associated to $\mathcal{E}$ and the second term is a regular part involving a principal value operator excluding an infinitesimal ellipsoid similar to $\mathcal{E}$ around $\underline{0}$ and the hessian (second-order tensor) of G_m [51]. Note that the shape of the ellipsoid is arbitrary in this expression provided that it is the same in the Eshelby tensor and the principal value definition.

From Eshelby [2], the second-order Green operator is known to obey to the following remarkable results [51]

$$\begin{cases} \forall \underline{x} \in \overset{\circ}{\mathcal{E}}, \quad \displaystyle\int_{\underline{x}' \in \mathcal{E}} \boldsymbol{\Gamma}_m(\underline{x} - \underline{x}') \, \mathrm{d}\Omega' = \boldsymbol{S}_m^{\mathcal{E}} \cdot \boldsymbol{k}_m^{-1} & \text{(F.2a)} \\ \forall \underline{x} \in \partial\mathcal{E}^+, \quad \displaystyle\int_{\underline{x}' \in \mathcal{E}} \boldsymbol{\Gamma}_m(\underline{x} - \underline{x}') \, \mathrm{d}\Omega' = \boldsymbol{S}_m^{\mathcal{E}} \cdot \boldsymbol{k}_m^{-1} - \boldsymbol{\Pi}_m(\underline{n}) & \text{(F.2b)} \end{cases}$$

where $\overset{\circ}{\mathcal{E}}$ denotes the interior of $\mathcal{E}$ and $\partial\mathcal{E}^+$ denotes the set of points which are located immediately on the external part of the boundary of $\mathcal{E}$. In the case of a uniform polarization vector within $\mathcal{E}$, (F.1) together with (F.2a) ensure the uniformity of the temperature gradient within $\mathcal{E}$ and the term $\boldsymbol{\Pi}_m(\underline{n})$ in (F.2b), where $\underline{n}$ corresponds to the outward unit normal vector at point $\underline{x}$, is consistent with the effect of the interfacial operator recalled in (E.3). The temperature gradient as well as the heat flux vector are therefore not expected to be uniform outside $\mathcal{E}$ even along $\partial\mathcal{E}^+$.

Considering the symmetrical roles played by $\underline{x}$ and $\underline{x}'$ in the Green kernel i.e. $\boldsymbol{\Gamma}_m(\underline{x} - \underline{x}') = \boldsymbol{\Gamma}_m(\underline{x}' - \underline{x})$, (F.2a) allows to simplify the average of $\underline{h}$ in (F.1) over the domain $\mathcal{E}$ including its interface (so that $\underline{x}'$ always remains interior with respect to the integration domain of $\underline{x}$ and (F.2a) can apply)

$$< \underline{h} >_{\mathcal{E}} = \underline{H} - \boldsymbol{S}_m^{\mathcal{E}} \cdot \boldsymbol{k}_m^{-1} \cdot < \underline{p} >_{\mathcal{E}} = \underline{H} + \boldsymbol{S}_m^{\mathcal{E}} \cdot \left(< \underline{h} >_{\mathcal{E}} + \boldsymbol{k}_m^{-1} \cdot < \underline{u} >_{\mathcal{E}} \right) \tag{F.3}$$

All the average operations over $\mathcal{E}$ in (F.3) have to be considered in the sense of distributions ([52], [53]) i.e. the temperature gradient and heat flux vector fields may contain Dirac terms even possibly located on the boundary $\partial\mathcal{E}$ of the ellipsoid which have to be taken into account in the averages. It is worth emphasizing the fact that (F.3) has been obtained whatever the actual law within $\mathcal{E}$, thanks to a reasoning initially based on an arbitrary polarization defined by $\underline{p} = -(\boldsymbol{k}_m \cdot \underline{h} + \underline{u})$. For example, if $\mathcal{E}$ is composed of a homogeneous material of conductivity $\boldsymbol{k}_{\mathcal{E}}$, the polarization tensor is $\underline{p} = (\boldsymbol{k}_{\mathcal{E}} - \boldsymbol{k}_m) \cdot \underline{h}$, which implies that the average $< \underline{h} >_{\mathcal{E}}$ from (F.3) is as expected equal to the uniform value (D.1). In this case, the uniformity of the solution can directly be obtained from (F.1) and an argument of unicity

(Eshelby problem of inhomogeneity).

A straightforward consequence of (F.3) is the consistency of the notion of equivalent conductivity with the classical Eshelby result. Indeed, whatever the conduction law distribution within $\mathcal{E}$, it is recalled that a tensor $\boldsymbol{k}^{eq}$ can be identified by (76). Then the introduction of (76) in (F.3) leads to

$$< \underline{h} >_{\mathcal{E}} = \left(\mathbf{1} + \boldsymbol{S}_m^{\mathcal{E}} \cdot \boldsymbol{k}_m^{-1} \cdot (\boldsymbol{k}^{eq} - \boldsymbol{k}_m) \right)^{-1} \cdot \underline{H} \tag{F.4}$$

which is none other than the counterpart of (D.1) and can be further used as an estimated concentration law in classical homogenization schemes (dilute, Mori-Tanaka, self-consistent...).

[1] L. Dormieux, D. Kondo, F.-J. Ulm, Microporomechanics, John Wiley & Sons, Ltd, Chichester, UK, 2006. doi:10.1002/0470032006.
URL http://doi.wiley.com/10.1002/0470032006

[2] J. D. Eshelby, The determination of the elastic field of an ellipsoidal inclusion, and related problems, Proc. R. Soc. Ser. A 241 (A) (1957) 376–396.

[3] Z. Hashin, The Elastic Moduli of Heterogeneous Materials, J. Appl. Mech. 29 (1) (1962) 143–150. doi:10.1115/1.3636446.
URL https://asmedigitalcollection.asme.org/appliedmechanics/article/29/1/143/424947/The-Elastic-Moduli-of-Heterogeneous-Materials

[4] R. M. Christensen, K. H. Lo, Solutions for effective shear properties in three phase sphere and cylinder models, J. Mech. Phys. Solids 27 (1979) 315–330.

[5] E. Hervé, A. Zaoui, n-layered inclusion-based micromechanical modelling, Int. J. Engng. Sci. 31 (1993) 1–10.

[6] A. E. H. Love, Treatise on mathematical theory of elasticity. 4th edition, A Treatise Math. Theory Elast. (1944) 643.
URL https://archive.org/details/atreatiseonmath01lovegoog

[7] M. Bornert, Morphologically representative pattern-based bounding in elasticity, J. Mech. Phys. Solids 44 (3) (1996) 307–331. doi:10.1016/0022-5096(95)00083-6.
URL https://linkinghub.elsevier.com/retrieve/pii/0022509695000836

[8] A. Zaoui, Structural morphology and constitutive behaviour of microheterogeneous materials, in: P. Suquet (Ed.), Contin. micromechanics, CISM, SpringerWienNewYork, Udine, Italy, 1997, pp. 291–347.

[9] F. Chen, A. Giraud, I. Sevostianov, D. Grgic, Numerical evaluation of the Eshelby tensor for a concave superspherical inclusion, Int. J. Eng. Sci. 93 (2015) 51–58. doi:10.1016/j.ijengsci.2015.04.007.
URL http://dx.doi.org/10.1016/j.ijengsci.2015.04.007https://linkinghub.elsevier.com/retrieve/pii/S0020722515000592

[10] F. Chen, I. Sevostianov, A. Giraud, D. Grgic, Evaluation of the effective elastic and conductive properties of a material containing concave pores, Int. J. Eng. Sci. 97 (2015) 60–68. doi:10.1016/j.ijengsci.2015.08.012.
URL http://dx.doi.org/10.1016/j.ijengsci.2015.08.012https://linkinghub.elsevier.com/retrieve/pii/S0020722515001299

[11] I. Sevostianov, F. Chen, A. Giraud, D. Grgic, Compliance and resistivity contribution tensors of axisymmetric concave pores, Int. J. Eng. Sci. 101 (2016) 14–28. doi:10.1016/j.ijengsci.2015.12.005.
URL http://dx.doi.org/10.1016/j.ijengsci.2015.12.005https://linkinghub.elsevier.com/retrieve/pii/S0020722515002050

[12] A. Adessina, J.-F. Barthélémy, F. Lavergne, A. Ben Fraj, Effective elastic properties of materials with inclusions of complex structure, Int. J. Eng. Sci. 119 (2017) 1–15. doi:10.1016/j.ijengsci.2017.03.015.
URL https://linkinghub.elsevier.com/retrieve/pii/S0020722517304809

[13] E. Hervé, Thermal and thermoelastic behaviour of multiply coated inclusion-reinforced composites, Int. J. Solids Struct. 39 (4) (2002) 1041–1058. doi:10.1016/S0020-7683(01)00257-8.
URL http://linkinghub.elsevier.com/retrieve/pii/S0020768301002578

[14] Z. Hashin, The Spherical Inclusion With Imperfect Interface, J. Appl. Mech. 58 (2) (1991) 444–449. doi:10.1115/1.2897205.
URL https://asmedigitalcollection.asme.org/appliedmechanics/article/58/2/444/391325/The-Spherical-Inclusion-With-Imperfect-Interface

[15] L. Dormieux, L. Jeannin, N. Gland, Homogenized models of stress-sensitive reservoir rocks, Int. J. Eng. Sci. 49 (5) (2011) 386–396. doi:10.1016/j.ijengsci.2010.12.010.
URL http://dx.doi.org/10.1016/j.ijengsci.2010.12.010https://linkinghub.elsevier.com/retrieve/pii/S0020722510002776

[16] E. Hervé-Luanco, Elastic behavior of composites containing multi-layer coated particles with imperfect interface bonding conditions and application to size effects and mismatch in these composites, Int. J. Solids Struct. 51 (15-16) (2014) 2865–2877. doi:10.1016/j.ijsolstr.2014.04.008.
URL https://linkinghub.elsevier.com/retrieve/pii/S0020768314001577

[17] A. Aboutajeddine, K. Neale, The double-inclusion model: a new formulation and new estimates, Mech. Mater. 37 (2-3) (2005) 331–341. doi:10.1016/j.mechmat.2003.08.016.
URL https://linkinghub.elsevier.com/retrieve/pii/S0167663604000870

[18] F. Dinzart, H. Sabar, S. Berbenni, Homogenization of multi-phase composites based on a revisited formulation of the multi-coated inclusion problem, Int. J. Eng. Sci. 100 (2016) 136–151. doi:10.1016/j.ijengsci.2015.12.001.
URL https://linkinghub.elsevier.com/retrieve/pii/S0020722515001937

[19] F. Dinzart, A. Jeancolas, N. Bonfoh, H. Sabar, M. Mihaluta, Micromechanical modeling of the multi-coated ellipsoidal inclusion: application to effective thermal conductivity of composite materials, Arch. Appl. Mech. 88 (11) (2018) 1929–1944. doi:10.1007/s00419-018-1418-2.
URL https://doi.org/10.1007/s00419-018-1418-2http://link.springer.com/10.1007/s00419-018-1418-2
[20] Y. Benveniste, T. Miloh, The effective conductivity of composites with imperfect thermal contact at constituent interfaces, Int. J. Eng. Sci. 24 (9) (1986) 1537–1552.
[21] T. Miloh, Y. Benveniste, On the effective conductivity of composites with ellipsoidal inhomogeneities and highly conducting interfaces, Proc. R. Soc. A Math. Phys. Eng. Sci. 455 (1999) 2687–2706. doi:10.1098/rspa.1999.0422.
[22] V. I. Kushch, Micromechanics of Composites, Elsevier, 2013. doi:10.1016/C2012-0-03565-X.
URL https://linkinghub.elsevier.com/retrieve/pii/C2012003565X
[23] A. Riccardi, F. Montheillet, A generalized self-consistent method for solids containing randomly oriented spheroidal inclusions, Acta Mech. 133 (1-4) (1999) 39–56. doi:10.1007/BF01179009.
URL http://link.springer.com/10.1007/BF01179009
[24] H. Duan, J. Wang, Z. Huang, Y. Zhong, Stress fields of a spheroidal inhomogeneity with an interphase in an infinite medium under remote loadings, Proc. R. Soc. A Math. Phys. Eng. Sci. 461 (2056) (2005) 1055–1080. doi:10.1098/rspa.2004.1396.
URL http://rspa.royalsocietypublishing.org/cgi/doi/10.1098/rspa.2004.1396
[25] V. I. Kushch, Elastic fields and effective stiffness tensor of spheroidal particle composite with imperfect interface, Mech. Mater. 124 (February) (2018) 45–54. doi:10.1016/j.mechmat.2018.06.001.
URL https://linkinghub.elsevier.com/retrieve/pii/S0167663618301054
[26] V. I. Kushch, Elastic ellipsoidal inhomogeneity with imperfect interface: Complete displacement solution in terms of ellipsoidal harmonics, Int. J. Solids Struct. 166 (2019) 83–95. doi:10.1016/j.ijsolstr.2019.02.007.
URL https://doi.org/10.1016/j.ijsolstr.2019.02.007https://linkinghub.elsevier.com/retrieve/pii/S0020768319300800
[27] H. Le Quang, G. Bonnet, Q.-C. He, Size-dependent Eshelby tensor fields and effective conductivity of composites made of anisotropic phases with highly conducting imperfect interfaces, Phys. Rev. B 81 (064203) (2010) 1–15. doi:10.1103/PhysRevB.81.064203.
[28] H. Le Quang, Q.-C. He, G. Bonnet, Eshelby's tensor fields and effective conductivity of composites made of anisotropic phases with Kapitza's interface thermal resistance, Philos. Mag. 91 (25) (2011) 3358–3392. doi:10.1080/14786435.2011.580286.
URL http://www.tandfonline.com/doi/abs/10.1080/14786435.2011.580286
[29] N. Bonfoh, C. Dreistadt, H. Sabar, Micromechanical modeling of the anisotropic thermal conductivity of ellipsoidal inclusion-reinforced composite materials with weakly conducting interfaces, Int. J. Heat Mass Transf. 108 (2017) 1727–1739. doi:10.1016/j.ijheatmasstransfer.2016.12.008.
URL http://dx.doi.org/10.1016/j.ijheatmasstransfer.2016.12.008https://linkinghub.elsevier.com/retrieve/pii/S0017931016314053
[30] N. Bonfoh, A. Jeancolas, F. Dinzart, M. Mihaluta, Effective thermal conductivity of composite ellipsoid assemblages with weakly conducting interfaces, Compos. Struct. 202 (December 2017) (2018) 603–614. doi:10.1016/j.compstruct.2018.03.019.
[31] N. Bonfoh, H. Sabar, Anisotropic thermal conductivity of composites with ellipsoidal inclusions and highly conducting interfaces, Int. J. Heat Mass Transf. 118 (2018) 498–509. doi:10.1016/j.ijheatmasstransfer.2017.10.103.
URL https://doi.org/10.1016/j.ijheatmasstransfer.2017.10.103https://linkinghub.elsevier.com/retrieve/pii/S0017931017325978
[32] C.-W. Nan, R. Birringer, D. R. Clarke, H. Gleiter, Effective thermal conductivity of particulate composites with interfacial thermal resistance, J. Appl. Phys. 81 (10) (1997) 6692–6699. doi:10.1063/1.365209.
[33] H. Duan, B. Karihaloo, Effective thermal conductivities of heterogeneous media containing multiple imperfectly bonded inclusions, Phys. Rev. B 75 (6) (2007) 064206. doi:10.1103/PhysRevB.75.064206.
URL https://link.aps.org/doi/10.1103/PhysRevB.75.064206
[34] V. Levin, M. Markov, Effective thermal conductivity of micro-inhomogeneous media containing imperfectly bonded ellipsoidal inclusions, Int. J. Eng. Sci. 109 (2016) 202–215. doi:10.1016/j.ijengsci.2016.09.012.
URL http://dx.doi.org/10.1016/j.ijengsci.2016.09.012https://linkinghub.elsevier.com/retrieve/pii/S002072251630502X
[35] H. Le Quang, Determination of the effective conductivity of composites with spherical and spheroidal anisotropic particles and imperfect interfaces, Int. J. Heat Mass Transf. 95 (2016) 162–183. doi:10.1016/j.ijheatmasstransfer.2015.11.085.
URL http://dx.doi.org/10.1016/j.ijheatmasstransfer.2015.11.085https://linkinghub.elsevier.com/retrieve/pii/S0017931015307183
[36] M. Cherkaoui, H. Sabar, M. Berveiller, Elastic composites with coated reinforcements: A micromechanical approach for nonhomothetic topology, Int. J. Eng. Sci. 33 (6) (1995) 829–843. doi:10.1016/0020-7225(94)00108-V.
URL https://linkinghub.elsevier.com/retrieve/pii/002072259400108V
[37] L. Dormieux, E. Lemarchand, S. Brisard, Equivalent Inclusion Approach for Micromechanics Estimates of Nanocomposite Elastic Properties, J. Nanomechanics Micromechanics 6 (2) (2016) 04016002. doi:10.1061/(ASCE)NM.2153-5477.0000104.
URL http://ascelibrary.org/doi/10.1061/{%}28ASCE{%}29NM.2153-5477.0000104
[38] F. Dinzart, H. Sabar, New micromechanical modeling of the elastic behavior of composite materials with ellipsoidal reinforcements and imperfect interfaces, Int. J. Solids Struct. 108 (2017) 254–262. doi:10.1016/j.ijsolstr.2016.12.024.
URL https://linkinghub.elsevier.com/retrieve/pii/S0020768316304097
[39] E. W. Hobson, The Theory of Spherical and Ellipsoidal Harmonics, Cambridge University Press, 1931.
[40] M. Abramowitz, I. A. Stegun, Handbook of Mathematical Functions, National Bureau of Standards - Applied Mathematics Series - 55, Washington D.C., 1972.
[41] G. Dassios, Ellipsoidal Harmonics, Cambridge University Press, Cambridge, 2012. doi:10.1017/CBO9781139017749.

URL http://ebooks.cambridge.org/ref/id/CBO9781139017749
[42] V. I. Kushch, I. Sevostianov, A. S. Belyaev, Effective conductivity of spheroidal particle composite with imperfect interfaces : Complete solutions for periodic and random micro structures, Mech. Mater. 89 (2015) 1–11. doi:10.1016/j.mechmat.2015.05.010.
[43] P. L. Kapitza, Heat Transfer and Superfluidity of Helium II, Phys. Rev. 60 (4) (1941) 354–355. doi:10.1103/PhysRev.60.354.
URL https://link.aps.org/doi/10.1103/PhysRev.60.354
[44] Y. Mikata, M. Taya, Stress Field in and Around a Coated Short Fiber in an Infinite Matrix Subjected to Uniaxial and Biaxial Loadings, J. Appl. Mech. 52 (1) (1985) 19. doi:10.1115/1.3168996.
URL http://appliedmechanics.asmedigitalcollection.asme.org/article.aspx?articleid=1407885
[45] J.-F. Barthélémy, Effective Permeability of Media with a Dense Network of Long and Micro Fractures, Transp. Porous Media 76 (1) (2009) 153–178. doi:10.1007/s11242-008-9241-9.
URL http://link.springer.com/10.1007/s11242-008-9241-9
[46] P. Ponte Castañeda, J. R. Willis, The effect of spatial distribution on the effective behavior of composite materials and cracked media, J. Mech. Phys. Solids 43 (12) (1995) 1919–1951.
[47] I. Sevostianov, On the shape of effective inclusion in the Maxwell homogenization scheme for anisotropic elastic composites, Mech. Mater. 75 (2014) 45–59. doi:10.1016/j.mechmat.2014.03.003.
URL http://dx.doi.org/10.1016/j.mechmat.2014.03.003
[48] F. Johansson, et al., mpmath: a Python library for arbitrary-precision floating-point arithmetic (version 0.19), http://mpmath.org/ (2015).
[49] J. Hadamard, Leçons sur la propagation des ondes et les équations de l'hydrodynamique (in French), Hermann, Paris, 1903.
[50] S.-T. Gu, Q.-C. He, Interfacial discontinuity relations for coupled multifield phenomena and their application to the modeling of thin interphases as imperfect interfaces, J. Mech. Phys. Solids 59 (7) (2011) 1413–1426. doi:10.1016/j.jmps.2011.04.004.
URL https://linkinghub.elsevier.com/retrieve/pii/S0022509611000664
[51] T. Mura, Micromechanics of Defects in Solids, Second Edition, Kluwer Academic, 1987. doi:10.1002/zamm.19890690204.
[52] L. Schwartz, Théorie des distributions (in French), Hermann, Paris, 1966.
[53] I. M. Gel'fand, G. E. Shilov, Generalized functions - Vol I Properties and Operations, Vol. 1, Academic press, New-York and London, 1964.